Southeastern Geology: Volume 29, No. 3 February 1989

Edited by: S. Duncan Heron, Jr.

Abstract

Academic journal published quarterly by the Department of Geology, Duke University.

SOUTHEASTERN GEOLOGY

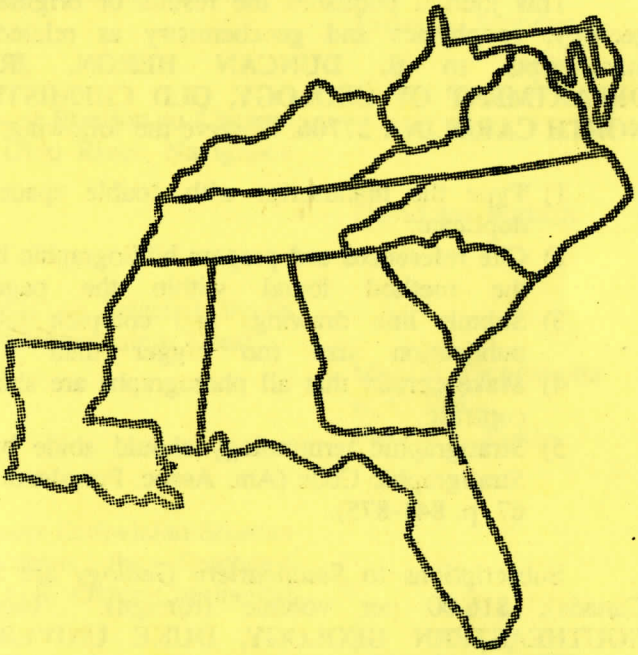

PUBLISHED AT DUKE UNIVERSITY DURHAM, NORTH CAROLINA

VOL. 29, NO. 3 FEBRUARY 1989

SOUTHEASTERN GEOLOGY

PUBLISHED QUARTERLY

AT

DUKE UNIVERSITY

Editor in Chief:
S. Duncan Heron, Jr.

Managing Editor:
James W. Clarke

This journal publishes the results of original research on all phases of geology, geophysics and geochemistry as related to the Southeast. Send manuscripts to **S. DUNCAN HERON, JR., DUKE UNIVERSITY, DEPARTMENT OF GEOLOGY, OLD CHEMISTRY BUILDING, DURHAM, NORTH CAROLINA 27706**. Observe the following:

1) Type the manuscript with double space lines and submit in duplicate.
2) Cite references and prepare bibliographic lists in accordance with the method found within the pages of this journal.
3) Submit line drawings and complex tables reduced to final publication size (no bigger than 8 x 5 1/8 inches).
4) Make certain that all photographs are sharp, clear, and of good contrast.
5) Stratigraphic terminology should abide by the North American Stratigraphic Code (Am. Assoc. Petroleum Geologists Bulletin, v. 67, p. 841-875).

Subscriptions to *Southeastern Geology* are $12.00 per volume (US and Canada), $16.00 per volume (foreign). Inquires should be sent to: **SOUTHEASTERN GEOLOGY, DUKE UNIVERSITY, DEPARTMENT OF GEOLOGY, OLD CHEMISTRY BUILDING, DURHAM, NORTH CAROLINA 27706**. Make checks payable to: *Southeastern Geology*.

SOUTHEASTERN GEOLOGY

Table of Contents

Vol. 29, No. 3

February 1989

HYDROGEOCHEMICAL ASPECTS OF GOLD IN THE WEATHERING ENVIRONMENT: IMPLICATIONS FOR POSSIBLE SECONDARY CONCENTRATION IN THE COASTAL PLAIN SEDIMENTS OF SOUTH CAROLINA

JAMES A. SAUNDERS

Dept. of Geology and Geological Engineering
University of Mississippi
University, MS 38677

ABSTRACT

Weathering of gold deposits generally produces mobilization of gold and reprecipitation on a local scale. Factors that affect the mobility of gold in the weathering environment include: climate, topography, rock composition and structure, Eh, pH, and the activities of dissolved chloride and sulfur species. The specific combination of these factors in the Piedmont and adjacent Coastal Plain provinces of southeastern U.S.A. suggests that regional mobilization of gold is possible. Weathering of either primary gold sources in crystalline rocks or secondary detrital sources in Cretaceous sediments could produce groundwater of enhanced gold solubility. Gold forms stable complexes with thiosulfate ($S_2O_3^{2-}$), which is a principal product of sulfide mineral oxidation. The gold-thiosulfate complex is most stable under slightly oxidizing and mildly acidic to mildly alkaline conditions. Hydrolysis reactions, such as the alteration of feldspar to clay, along with rapid groundwater flushing, probably buffer the pH to the required range for enhanced gold solubility under subtropical conditions.

Mobilization of gold out of the immediate site of weathering leads to the possibility of reprecipitation to form economic concentrations away from the source. One environment that appears favorable for reprecipitation is the basal Cretaceous aquifer overlying the Carolina slate belt in South Carolina. Groundwater, possibly containing elevated gold concentrations from the weathering of gold-pyrite deposits or disseminations in the slate belt, should recharge the overlying aquifer near the Fall Line. Dissolution of detrital gold could further enhance gold solubility in groundwater, and precipitation should occur at a redox boundary in the aquifer.

INTRODUCTION

Numerous pyrite-bearing gold deposits and prospects occur within the Carolina slate belt adjacent to the unconformable contact with the Cretaceous and younger sediments of the Coastal Plain (Figure 1). This observation led Saunders (1988) to propose that the weathering of gold-pyrite bodies or disseminations in this unique hydrogeologic setting could produce secondary concentrations of gold. The general hydrogeologic aspects of groundwater flow in the vicinity of the contact between the Cretaceous sediments and the slate belt crystalline rocks as a

possible ore-forming environment were discussed in Saunders (1988). This study presents hydrogeochemical aspects of gold mobility interpreted for a humid subtropical climate, including the geochemical aspects favoring gold transport and deposition in aquifers within Coastal Plain sediments.

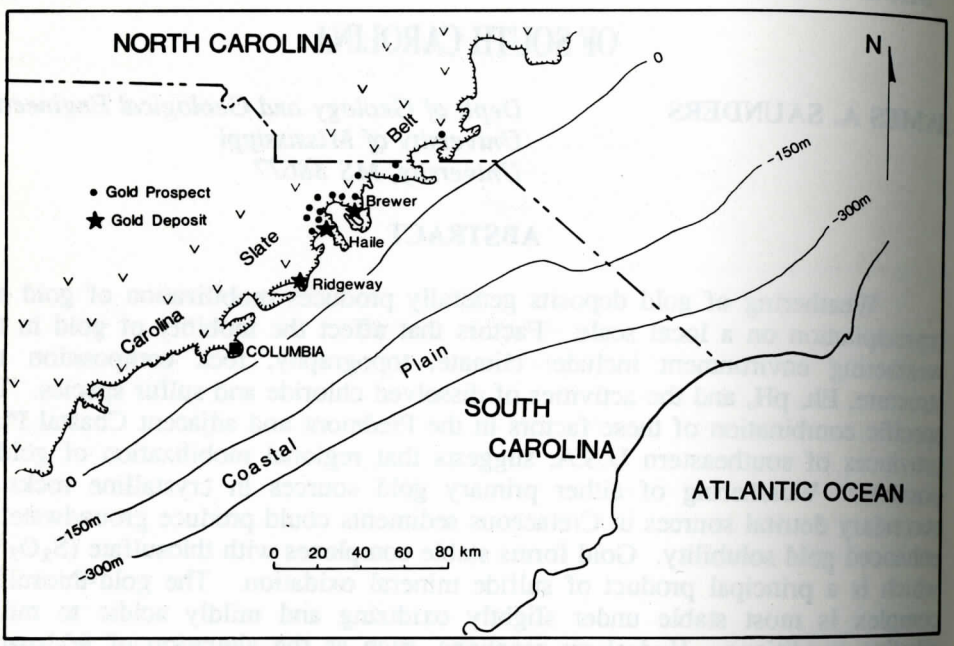

Figure 1. Map showing the location of gold deposits and prospects in relation to the contact between the Carolina slate belt and the Cretaceous sediments of the Coastal Plain (hachured line). Contours show the elevation of the pre-Cretaceous basement, from Bonini and Woolard (1960).

GEOCHEMISTRY OF GOLD IN THE WEATHERING ENVIRONMENT

Experimental studies conducted to determine the solubility of gold and silver in solutions approximating surface waters and hydrothermal solutions are summarized by Boyle (1979). From these studies, it is apparent that Au and Ag solubility is greatly enhanced by the presence of ligands capable of forming aqueous complexes with the precious metals, in particular, complexes with chloride or sulfur-bearing ligands (Barnes, 1979). When present in significant quantities, chloride forms stable complexes with gold at low pH under very oxidizing conditions (Krauskopf, 1951; Cloke and Kelly, 1964), and with silver in mildly oxidizing to oxidizing, low pH conditions (Mann, 1984). Reduced sulfur-bearing ligands, such as bisulfide (HS^-), form stable complexes with gold in neutral to alkaline, reducing solutions (Seward, 1973), and with silver (Sillen and Martell, 1971) probably under similar conditions. Sulfur-bearing ligands of intermediate oxidation state such as thiosulfate ($S_2O_3^{2-}$) form stable complexes with both gold and silver under mildly oxidizing, slightly acidic to alkaline conditions (Webster, 1986). In addition, organic ligands, most notably cyanide (CN^-), form stable

Table 1. Summary of Studies Involving the Weathering of Gold Deposits.

Location	Terrain/ Climate	Host Rocks	Groundwater Geochemistry	Interpreted Precious Metal Mobility	Reference
Summitville, CO	Alpine, semi-arid	felsic stock	Low pH, oxidizing, low chloride sulfate = 500 ppm	Au and Ag locally mobilized as thisosulfate complexes, reprecipitated locally	Stoffregen (1986)
Edna May mine and other examples from Yilgarn Block Western Australia	low relief arid to semi-arid lateritic environment	granite greenstone	low pH, oxidizing, chloride = 1000, 10,000 ppm sulfate = 200-900 ppm	Au, Ag mobilized as chloride complexes, Au of high fineness preferentially reprecipitated by reduction on Fe-hydroxides	Mann (1984); Webster and Mann (1984)
Upper Ridges Mine Wau, Papua, New Guinea	Extreme relief; sub-tropical climate	hydrothermal breccias carbonate lodes	neutral pH, oxidizing low chloride	Au, Ag mobilized as thiosulfate complexes, reprecipitation by oxidation and reduction to form electrum of low fineness	Webster and Mann (1984)
Calhoun Mine Limpkin County, GA	low to moderate relief; sub-tropical climate	Schist gneiss	no data	gold mobilized with ferrous Fe?	Kinkel and Lesure (1986) Lesure (1971)
Sleeper Mine Humboldt County, NV	Desert, arid	ashflow tuffs	pH=7.7-8.1 oxidizing, Cl=140-280 ppm sulfate=110-280 ppm	Au immobile, Ag mobilized as chloride complexes	Saunders and others (1988) and unpublished data

complexes with gold under a wide range of geochemical conditions at low temperatures (Boyle, 1979).

Recent studies of precious metal distribution in different weathering environments (Lakin and others, 1974; Mann, 1984; Webster and Mann, 1984; Stoffregen, 1986; and Saunders and others, 1988) show that the aqueous geochemical data are consistent with observed trends in gold and silver depletion or enrichment. In addition, these studies have suggested a number of geochemical and hydrogeologic factors that apparently control precious metal mobility in the weathering environment. These include: climate, topography, host rock composition and structure, Eh, pH, and the activities of dissolved chloride and sulfur species. These studies indicate that combinations of these factors lead to differences in the relative mobility of gold and silver (Table 1).

Of particular interest to this study are the conditions under which gold can be mobilized and transported out of the immediate site of weathering and potentially reprecipitated in economic concentrations. Mobilization of gold as chloride complexes requires unique geochemical conditions at surface temperatures, such as exhibited by the chloride-rich, oxidizing, and low-pH waters produced in lateritic environments (Mann, 1984). Under these conditions, gold is transported only locally because reprecipitation is caused by reduction (Mann, 1984), or also quite probably by dilution and buffering away from the site. Solubility of gold under reducing conditions is controlled by the activities of H_2S (aq) and HS^- (Webster, 1986). The activity of these reduced-sulfur ligands is primarily controlled by the solubility of iron-sulfide minerals, which is very low at surface temperature. Under the mildly oxidizing, slightly alkaline conditions produced by the weathering of precious metal-bearing carbonate-sulfide lodes at Wau, New Guinea, both gold and silver are mobilized as thiosulfate complexes (Webster and Mann, 1984; Webster, 1986). In this environment, the presence of carbonate minerals buffers the groundwater pH to the neutral range required to stabilize thiosulfate and mobilize gold. This process was predicted by Lakin and others (1974) from the interpretation of their laboratory results on the leaching of gold by thiosulfate solutions.

Thiosulfate, and the related species sulfite (SO_3^{2-}), are metastable intermediaries between sulfide and sulfate. However at low temperature, the slow kinetics of the inorganic sulfur redox reactions allow the continued existence of these species, apparently almost indefinitely under subsurface conditions. Experimental data indicate that thiosulfate is the predominant sulfur species formed by the oxidation of sulfides (Granger and Warren, 1969; Goldhaber, 1983; and Moses and others, 1987). In addition, other studies have indicated that thiosulfate persists under hydrothermal conditions (Giggenbach, 1974; Ohmoto and Lasaga, 1982), and may contribute to the formation of some types of relatively low-temperature hydrothermal ore deposits (Barnes, 1979; Boyle, 1979; and Spirakis, 1986). Webster (1986) reviewed the available thermochemical data for gold solubility in solutions containing potentially significant ligands, and calculated the solubility of gold expected in the mildly oxidizing, sulfur-rich groundwater in the immediate vicinity of a weathering sulfide-gold deposit (Figure 2). In this environment at neutral pH, gold is quite soluble and exists primarily as $Au(S_2O_3)_2^{3-}$.

Little data exist on the abundance of thiosulfate in natural waters (Webster,

1987). This is due to the fact that it is not routinely determined in standard water analyses, and because of the rapid oxidation to sulfate by atmospheric oxygen. Because of the latter, a significant portion of sulfate reported for groundwaters could have been derived from thiosulfate.

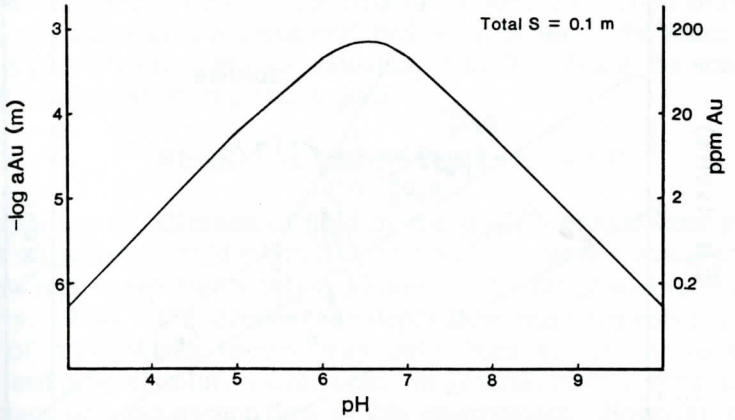

Figure 2. Solubility of gold interpreted for the immediate site of weathering under mildly oxidizing conditions, modified from Webster (1986).

From the recent studies, it is apparent that gold mobilization by thiosulfate is probable under mildly oxidizing conditions buffered to the neutral pH range, as occurs at Wau, New Guinea. However, other environments can produce the necessary Eh-pH-compositional conditions required for mobilizing gold as a thiosulfate complex. Weathering of gold-bearing pyritic bodies or disseminations in crystalline rocks under subtropical conditions may also be favorable (Saunders, 1988). In this environment, rapid groundwater flushing due to relatively high annual rainfall and hydrolysis reactions, such as the alteration of feldspar to clay, tend to buffer the groundwater pH to the neutral range (Freeze and Cherry, 1979). Limited observations on gold mobility in the weathering environment in the southeastern U.S.A. suggest that the proper Eh-pH conditions might exist locally. For example, Kinkel and Lesure (1968) and Lesure (1971) observed the coprecipitation of gold and "limonite" by groundwater flowing through fractures in underground workings at the abandoned Calhoun mine, Lumpkin County, Georgia, and at other locations. This implies that gold is mobilized along with ferrous iron, and both appear to precipitate in response to oxidation in the mine workings.

Figure 3 shows the equilibrium stability field for ferrous iron as a function of Eh and pH with respect to pyrite and goethite for a typical groundwater. In addition, by using the data of Webster (1986) the approximate area for maximum gold solubility as a thiosulfate complex can also be shown. Path A represents a sequence of events consistent with the observations of Kinkel and Lesure (1968) and Lesure (1971), where 1) pyrite is oxidized in the neutral pH range; 2) ferrous iron and gold are dissolved; and 3) subsequent oxidation causes coprecipitation of goethite and gold. For a groundwater with low chloride content under the general conditions depicted by Path A, gold solubility would appear to be controlled by thiosulfate. Similar geochemical conditions could be responsible for the formation of at least some of the alluvial gold nuggets in the Piedmont of the

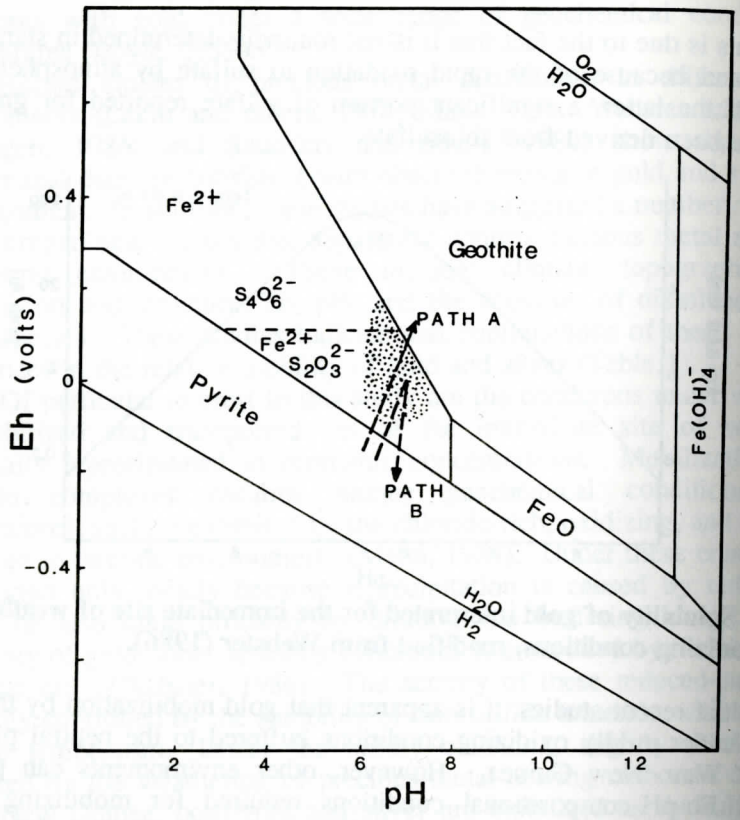

Figure 3. Eh-pH diagram for a typical groundwater calculated for 0.001M sulfur, and 0.5 ppm iron, from Hem (1985). Data for the stability fields of the sulfur species of intermediate oxidation state are from Webster (1986). Dotted area shows conditions of maximum gold solubility as a thiosulfate complexes.

southeastern U.S.A. In this scenario, oxidation of pyrite in gold-bearing rocks allows the formation of gold-thiosulfate complexes that migrate toward stream valleys as part of the topographically-controlled shallow groundwater regime. Oxidation of the gold-thiosulfate complex in the active stream channel would then cause gold precipitation. The formation of nuggets by accretion or by residual accumulation is a source of great debate, yet clearly the delicate dendritic and crystalline gold morphologies present in active stream channels, most recently described by Cook (1987), must result from the aqueous transport of gold.

Most gold production from Alabama and Georgia has come from gold present in saprolite locally enriched above values for the less-weathered underlying bedrock or veins (Pardee and Park, 1948; Lesure, 1971; Paris, 1985; Cook, 1987). In many cases, gold appears to be concentrated at the bedrock/saprolite interface or at the water table. Elevated gold content of saprolite is generally believed to be the result of residual accumulation as erosion progresses, although local concentrations in saprolite might be caused by lateral groundwater flow in the shallow regime. In the latter situation, gold would precipitate as more reducing conditions are encountered, for reduction is an effective precipitation mechanism

for gold complexed by thiosulfate (Webster and Mann, 1984). Path B (Figure 3) illustrates this interpreted sequence of events.

In general, the details of the supergene distribution of gold in the historic deposits of the Southeast with respect to present or past groundwater conditions are not well documented. Although the bulk of the gold production from this region was from residually- or supergene-enriched ore at or above the water table (Cook, 1987), it is possible that a gradual oxidation of sulfides below the water table may also result in dissolution of primary gold.

REGIONAL TRANSPORT OF GOLD

The apparent mobilization of gold by the shallow groundwater system in the Southeast suggests that gold might be mobilized on a more regional scale, because the shallow regime represents only a portion of the total groundwater flow (Freeze and Cherry, 1979). The intermediate-depth flow regime involves much greater volumes of rock, which locally may have been susceptible to slow sulfide oxidation and gold dissolution over time. In general, there is little data available on the details of groundwater flow in this environment. However, one situation where flow conditions can be predicted is in the vicinity of the unconformable contact between the crystalline rocks of the Carolina slate belt and the Cretaceous sediments of the Coastal Plain. This contact is generally referred to as the "Fall Line" because of the elevation drop going from the crystalline rocks to the Coastal Plain sediments. Because of the gradual dip of the contact, the overlying sediments, and the ground surface towards the coast, groundwater from the crystalline rocks should recharge the basal Coastal Plain aquifer in the vicinity of the contact (Figure 4). The existence of numerous gold-pyrite deposits and prospects near this contact, ant the probability that the slate belt rocks may host additional deposits or disseminations beneath the Coastal Plain sediments, suggest the potential for an ore-forming system in this environment.

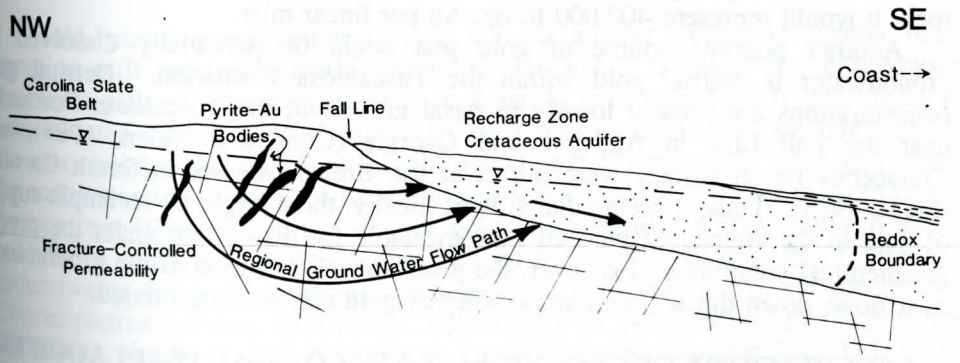

Figure 4. Interpreted groundwater flow conditions at the Piedmont-Coastal Plain contact.

The general features of the proposed model include: 1) dissolution of gold from local primary deposits or regional disseminations by the oxidation of sulfides to form thiosulfate; 2) flow of groundwater into the basal Coastal Plain aquifer; 3)

down dip flow in the aquifer, and 4) precipitation of gold at a redox boundary by reduction of the thiosulfate complex. The proposed model is similar in a number of respects to the geochemical and hydrologic environment of uranium mobilization and precipitation in "roll-front" deposits of southeastern Texas. In southeastern Texas, uranium is leached out of the volcaniclastic Catahoula Formation by oxidizing groundwater, which flows into an overlying semi-confined to confined aquifer, and uranium precipitates at a redox boundary (Galloway, 1977).

The hydrogeology of the crystalline rock-Cretaceous sediment contact has been extensively studied in the vicinity of the Savannah River Plant of the U.S. Department of Energy near Aiken, South Carolina (Siple, 1964; 1967). The site lies approximately 900 feet above the contact. Four deep holes were drilled to investigate the hydrogeology of the crystalline rocks to evaluate their potential for hosting a radioactive waste storage facility (Siple, 1964). Fractures in the crystalline rocks extend down 400-500 feet below the contact and contained brackish groundwater predominantly composed of sodium and sulfate with a pH of 8-9. Groundwater in the fractures exhibits artesian head because a clay-rich saprolite layer serves to confine the groundwater in the crystalline rocks at this depth. At shallower depths, the saprolite is discontinuous, and groundwater in the crystalline rocks is hydraulically connected with the overlying Tuscaloosa Formation (Siple, 1964). Groundwater in the unconfined portion of the fracture-controlled aquifer and the overlying Cretaceous formations is slightly acidic and fresher than the deeper groundwater in the crystalline rocks (Siple, 1967).

By estimating a depth of 500 feet as the point at which the groundwaters in the crystalline rocks become confined, and using a regional dip of 35 feet/mile (Siple, 1964) for the unconformity, then recharge into the Tuscaloosa Formation from the slate belt rocks occurs over a lateral distance of approximately 14 miles in the vicinity of the Savannah River Plant. This corresponds to approximately 1.3 cubic miles of crystalline rocks involved in this intermediate groundwater flow system per linear mile using reasonable assumptions about depths of groundwater circulation. If 1 part per billion (ppb) of gold was leached from this volume of rock, it would represent 400,000 tr. oz. Au per linear mile.

Another possible source of gold that could be potentially dissolved by groundwater is detrital gold within the Tuscaloosa Formation. Detrital gold concentrations are present locally in basal gravels in the Tuscaloosa Formation near the Fall Line in Alabama and Georgia (Cook and Nelen, 1988), and Cretaceous beach placers were mined at the Brewer deposit in South Carolina (Feiss, 1985). Thus, it seems that at least locally, there might be an ample supply of gold in the vicinity of the Fall Line available for dissolution under the proper geochemical conditions. However, the geochemical evolution of the groundwater as it flows down dip will determine whether gold can be concentrated.

GEOCHEMISTRY OF GROUNDWATER IN COASTAL PLAIN AQUIFERS

Groundwater in confined aquifers typically becomes more reducing with depth (Freeze and Cherry, 1979). Broom (1966) proposed that this decrease in oxidation potential can explain the high iron content of many aquifers in the Coastal Plain of Texas. More recently, Lee (1985) observed a general redox zonation in

Cretaceous Coastal Plain aquifers in Mississippi and Alabama. Lee developed a model for the geochemical evolution of groundwater in these aquifers using water chemistry from wells along several flow paths in conjunction with quantitative computer speciation and mass balance programs. Lee recognized 4 principal zones based on the groundwater geochemistry (Figure 5). These zones are defined principally by water-mineral reactions, and to a lesser extent, organic reactions. The zones include: the uppermost Zone A, which is very oxidizing, and dissolved oxygen from the atmosphere is gradually consumed by the oxidation of organic matter; Zone B, which is less oxidizing, where iron is present in the ferrous state and is locally abundant due to the dissolution of ferric iron minerals; Zone C, variably present depending on aquifer mineralogy, where dissolution of calcite, aided by cation exchange of Ca for Na in clay minerals, increases bicarbonate activity, resulting in the precipitation of siderite; and Zone D, where bacterial reduction of sulfate to sulfide causes pyrite precipitation and lowers the iron content of the groundwater significantly. The scale of this zonation is variable and is dependent on the local hydrogeologic and geochemical conditions.

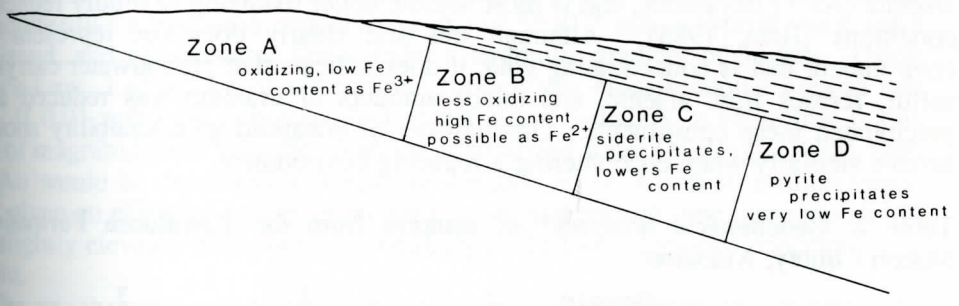

Figure 5. Geochemical zonation observed in Mississippi-Alabama Cretaceous Coastal Plain aquifers, modified from Lee (1985).

Gold-bearing groundwater issuing into an aquifer exhibiting similar redox zonation will react differently depending on where it enters the groundwater evolution path. If the entry point is in Zone A, gold would likely precipitate on disseminated Fe-Mn oxyhydroxides by oxidation of the thiosulfate complex. If the entry point is in Zones B or C, gold would probably remain in solution, because the redox stability of the gold-thiosulfate complex at neutral pH is similar to that of ferrous iron (Figure 3). Any detrital gold in the aquifer within Zones B and C potentially could be dissolved depending on the activity of thiosulfate. Flow of groundwater down dip continues, and at Zone D, authigenic pyrite precipitates. Coprecipitation of gold with pyrite is likely due to the reduction of the sulfur in thiosulfate, similar to Path B in Figure 3. Groundwater entering Zone D from the crystalline rocks should undergo a similar reduction and precipitation of gold at the entry point.

The presence of authigenic pyrite in Cretaceous aquifers and formations of the Coastal Plain apparently is relatively common (see Siple, 1967; Lee, 1985). For example, authigenic pyrite is exposed in outcrops of the Tuscaloosa Formation along Uphapee Creek, approximately 1 mile northeast of Tuskegee, Alabama.

There, nodules of silver-colored pyrite (confirmed by x-ray diffraction) up to several cm in diameter have formed by the replacement of carbonitized root and wood fragments that occur in fluvial gravel deposits. The wood is locally silicified, and textural evidence indicates that this process was contemporaneous with pyritization. The geologic setting and textural evidence suggest that pyritization and silicification were post-depositional events, most probably caused by groundwater chemical processes. Because the geochemical conditions for pyrite formation here are similar to those for the Zone C-D interface, samples of the pyrite, silicified carbonitized wood, and "hard pan" formed from the oxidation of pyrite were analyzed for a selected suite of elements (Table 2). The samples have gold contents that are only slightly elevated compared to the crustal abundance of 4 ppb (Mason and Moore, 1982), but other trace elements are present elevated concentrations and provide some additional insight into the formative geochemical processes. For example, the silicified wood sample contains 14.6 ppm uranium as compared to a crustal abundance of 1.8 ppm, consistent with the fact that uranium precipitates from oxidizing groundwater by reduction. In addition, the pyrite sample contains 520 ppm arsenic, which probably imparts the silver color to it. Arsenic occurs in natural waters as either the arsenate (As^{5+}) or arsenite (As^{3+}) oxyanions, and is most soluble under oxidizing to mildly reducing conditions (Hem, 1985). Although this site clearly does not represent an environment that is concentrating gold, it does indicate that groundwater carrying sulfur, ferrous iron, arsenic, and minor amounts of uranium was reduced and precipitated these constituents. Groundwater of enhanced gold solubility should behave similarly when encountering a reducing environment.

Table 2. Geochemical analyses* of samples from the Tuscaloosa Formation, Macon County, Alabama

Sample	1	2	3
Ag ppm	<10	<5	<5
As ppm	520	4	<2
Au ppb	7	8	8
Ba ppm	<100	200	100
Ca %	<1	1	<1
Co ppm	100	<5	<5
Fe %	36.9	20.8	0.26
Mo ppm	120	<5	<5
Na %	<0.05	<0.05	<0.05
Se ppm	<5	<5	<5
Th ppm	2.5	3.5	<0.05
U ppm	1.1	7.7	14.6
Zn ppm	<50	<50	<50

Sample 1. Pyrite nodule with wood and root fragments
Sample 2. Massive iron oxy-hydroxides formed by pyrite oxidation
Sample 3. Silicified and carbonitized wood fragment

*Analyses conducted by instrumental neutron activation by Nuclear Activation Services, Hamilton, Ontario.

DISCUSSION AND CONCLUSIONS

Data on the gold content of groundwater is fairly limited (Boyle, 1979), and much of the published information may be in error because of earlier unreliable analytical procedures or improper sample preparation procedures (McHugh, 1988). Particulate or colloidal material enhances the apparent gold content of natural waters, and for that reason, should be carefully filtered (McHugh, 1988). Gold content of filtered water samples was determined by McHugh (1988), and he found generally lower values than reported in the literature. The mean value of gold in groundwater from springs was 0.003 ppb, whereas surface and groundwaters associated with, or in the vicinity of, known gold mineralization have a mean gold content of 0.101 ppb (McHugh, 1988).

Given the high potential solubility of gold in mildly oxidizing to mildly reducing conditions in the presence of sulfur species of intermediate oxidation state, gold contents in the 0.0X ppb range could be expected in the vicinity of the Fall Line due to the dissolution of primary or detrital gold. Example calculations suggest that precipitation of gold from such solutions could potentially produce significant concentrations. For example, assume that a 300m by 10m cross-sectional area is representative of a redox boundary in an aquifer at one location. The aquifer has a hydraulic conductivity (K) of $5*10^{-4}$ m/s, a typical value for a clean sand, and groundwater flows under a hydraulic gradient of 3m/km. Using Darcy's Law, $1.4*10^{8}$ kg of water flow through this cross-sectional area in one year. If 0.01 ppb gold is precipitated at the redox boundary, a value that is one order of magnitude less than the mean for mineralized water (McHugh, 1988), then 1.4g Au would be deposited in a year, or 450,000 tr. oz. Au in 10 million years. Thus, given an effective precipitation mechanism and enough time, groundwater of only slightly elevated gold content potentially could form economic concentrations of gold.

The geochemical and hydrologic arguments presented here do not prove the existence of secondary gold accumulations in Coastal Plain sediments. However, the formation of roll-front uranium deposits in the Coastal Plain and elsewhere proves that groundwater systems can precipitate economic concentrations of at least some elements. Why not gold? Currently, exploration for primary gold deposits in the Carolina slate belt "basement" beneath the Cretaceous cover is taking place. The present study suggests that the overlying sediments should not be neglected. If these deposits do exist, then they have the potential for low cost exploitation using in-situ leaching similar to that utilized in the southeast Texas uranium deposits. Concentrated thiosulfate solutions could be used to leach gold with no adverse environmental effects.

ACKNOWLEDGEMENTS

Discussions with Bob Carpenter, Bob Cook, Sam Romberger, Jenny Webster, and Don Baker were helpful in clarifying certain aspects of this paper. Earlier versions of the manuscript were reviewed by Terry Klein, Henry Bell, Paul Stout, and an anonymous reviewer. Their input provided additional insights and improved the manuscript significantly. Western Mining Corporation (USA) provided financial support for the geochemical analyses.

REFERENCES CITED

Barnes, H.L., 1979, solubilities of ore minerals, in Barnes, H.L. (ed.), Geochemistry of Hydrothermal Ore Deposits: New York, John Wiley and Sons, p. 404-460.

Bonini, W.E., and Woolard, G.P., 1960, Subsurface geology of North Carolina-South Carolina Coastal Plain from seismic data: American Association of Petroleum Geologists Bulletin, v. 44, p. 298-315.

Boyle, R.W., 1979, The geochemistry of gold and its deposits: Geological Survey of Canada Bulletin 280.

Broom, M.E., 1966, "Iron Water" from wells: causes and prevention: Ground Water, v. 4, p. 18-21.

Cloke, P.C., and Kelly, W.C., 1964, Solubility of gold under inorganic supergene conditions: Economic Geology, v. 59, p. 259-270.

Cook, R.B. Jr., 1987, Notable occurrences of gold in Georgia and Alabama: Mineralogical Record, v. 18, no. 1, p. 65-74.

Cook, R.B. Jr., and Nelen, J.A., 1988, Exploration significance of multistage Cretaceous and modern processes in gold placers of the Georgia-Alabama Fall Line: Society of Mining Engineers of A.I.M.E. Preprint number 88-2, 7p.

Feiss, P.G., 1985, Gold mineralization in the Carolina Slate Belt: Speculations on ore genesis, in Misra, K.C., (ed.), Volcanogenic Sulfide and Precious Metal Mineralization in the Southern Appalachians: University of Tennessee Dept. of Geological Sciences Studies in Geology 16, p. 220-236.

Freeze, R.A., and Cherry, J.A., 1979, Groundwater: Englewood Cliffs, NJ, Prentice-Hall, 604 p.

Galloway, W.E., 1977, Catahoula Formation of the Texas Coastal Plain: Depositional systems, composition, structural development, groundwater flow history and uranium deposition: Bureau of Economic Geology, University of Texas-Austin, Report of Investigation 87, 59 p.

Giggenbach, W.F., 1974, Kinetics of the polysulfide-thiosulfate disproportionation up to 240° C: Inorganic Chemistry, v. 13, p. 1730- 1733.

Goldhaber, M.B., 1983, Experimental study of metastable sulfur oxy-anion formation during pyrite oxidation at pH 6-9 at 30° C: American Journal of Science, v. 283, p. 193-217.

Granger, H.C., and Warren, C.G., 1969, Unstable sulfur compounds and the origin of roll-type uranium deposits: Economic Geology, v. 64, p. 160- 171.

Hem, J.D., 1985, Study and interpretation of chemical characteristics of natural water: U.S. Geological Survey Water Supply Paper 2254, 264 p.

Kinkel, A.R. Jr., and Lesure, F.G., 1969, Residual enrichment and supergene migration of gold, southeastern United States: U.S. Geological Survey Professional Paper 600-D, p. D174-D178.

Krauskopf, K.B., 1951, The solubility of gold: Economic Geology, v. 46, p.858-870.

Lakin, H.W., Curin, G.C., Hubert, A.E., Shacklette, H.T., and Doxtader, G., 1974, Geochemistry of gold in the weathering cycle: U.S. Geological Survey Bulletin 1330, 80 p.

Lee, R.W., 1985, Geochemistry of groundwater in Cretaceous sediments of the southeastern Coastal Plain of eastern Mississippi and western Alabama:

Water Resources Research, v. 21, p. 1545-1556.
Lesure, F.G., 1971, Residual enrichment and supergene transport of gold, Calhoun Mine, Lumpkin County, Georgia: Economic Geology, v. 66, p. 178-186.
McHugh, J.B., 1988, Concentration of gold in natural waters: Journal of Geochemical Exploration, v. 30, p. 85-94.
Mann, A.W., 1984, Mobility of gold and silver in lateritic weathering profiles: some observations from western Australia: Economic Geology, v. 79, p. 38-49.
Mason, B., and Moore, C.B., 1982, Principles of geochemistry: John Wiley and Sons, New York, 344 p.
Moses, C.O., Nordstrom, D.K., Herman, J.S., and Mills, A.C., 1987, Aqueous pyrite oxidation by dissolved oxygen and ferric iron: Geochimica et Cosmochimica Acta, v. 51, p. 1561-1572.
Ohmoto, H., and Lasaga, A.C., 1982, Kinetics of reactions between aqueous sulfates and sulfides in hydrothermal systems: Geochimica et Cosmochimica Acta, v. 46, p. 1727-1745.
Paris, T.A., 1985, The Goldville project: results of an exploration project for gold in the northern Alabama Piedmont, *in* Misra, K.C. (ed.), Volcanogenic Sulfide and Precious Metal Mineralization in the Southern Appalachians: University of Tennessee Dept. of Geological Sciences Studies in Geology 16, p. 182-204.
Pardee, J.T., and Park, C.F. Jr., 1948, Gold deposits of the southern Piedmont: U.S. Geological Survey Professional Paper 213, 156 p.
Saunders, J.A., 1988, Weathering of gold- and pyrite-bearing rocks as a source of gold for secondary deposits: Geological Society of Australia Abstract Series, V. 23, p. 640-642.
Saunders, J.A., Utterback, W.C., Day, W.E., and Christian, R., 1988, Characteristics of bonanza epithermal gold mineralization at the Sleeper deposit, Nevada, USA: Geological Society of Australia Abstract Series v. 23, p. 386-388.
Seward, T.M., 1973, Thio complexes of gold and the transport of gold in hydrothermal solutions: Geochimica et Cosmochimica Acta, v. 37, p. 379-399.
Sillen, L.G., and Martell, A.E., 1971, stability constants of metal-ion complexes- Supplement No. 1: London Chemical Society Special Publication 25, 865 p.
Siple, G.E., 1964, Geohydrology of storage of radioactive waste in crystalline rocks of the AEC Savannah River Plant, South Carolina: U.S. Geological Survey Professional Paper 501-C, p. C180-C184.
Siple, G.E., 1967, Geology and groundwater of the Savannah River Plant and vicinity: U.S. Geological Survey Water Supply Paper 1841, 113 p.
Spirakis, C.S., 1986, The valence of sulfur in disulfides- an overlooked clue to the genesis of Mississippi Valley-Type lead-zinc deposits: Economic Geology, v. 81, p. 1544-1545.
Stoffregen, R., 1986, Observations on the behavior of gold during supergene oxidation at Summitville, Colorado, U.S.A., and implications for electrum stability in the weathering environment: Applied Geochemistry, v. 1, p. 549-558.

Webster, J.G., 1986, The solubility of gold and silver in the system Au-Ag- S-O_2-H_2O and 1 atm.: Geochimica et Cosmochimica Acta, v. 50, p. 1837-1845.

Webster, J.G., 1987, Thiosulfate in surficial geothermal waters, North Island, New Zealand: Applied Geochemistry, v. 2, p. 579-584.

Webster, J.G., and Mann, A.W., 1984, The influence of climate, geomorphology and primary geology on the supergene migration of gold and silver: Journal of Geochemical Exploration, v. 22, p. 21-42.

THE RELATION OF THALWEG POSITION TO CHANNEL CURVATURE ALONG THE OHIO RIVER, NAVIGATION MILE 633 TO 715

DAVID JON FURBISH *Department of Geology, Florida State University Tallahassee, Florida 32306*

ABSTRACT

The asymmetric velocity distribution that characterizes the flow field in a river bend originates with acceleration induced by the channel curvature. Along two reaches of the Ohio River, this influence of curvature appears as a systematic displacement of the thalweg from the channel centerline. This displacement is related theoretically to channel curvature by a linear convolution. Once cast in the form of a linear difference equation, the convolution form is confirmed using Box-Jenkins-style time series analysis. This relation of thalweg position to channel curvature illustrates how curvature — because it does not change quickly — exerts a persistent influence on the flow field, and on the transient evolution of bed forms that are much smaller than a bend.

INTRODUCTION

A curved river channel induces a centrifugal acceleration of the flowing water. This leads to an asymmetric flow field wherein highest reach velocities are displaced toward the outside bank and secondary convective currents are driven by a superelevated water surface. This flow field governs erosion and movement of sediment within the channel, so it is reasonable to expect that evolution of channel forms, including the meandering process, can be related directly to channel curvature. This view is supported by field evidence (Hickin, 1974; Hickin and Nanson, 1975; Odgaard, 1987) and by theoretical work (Apmann, 1972; Allen, 1977; Begin, 1981; Parker and others, 1983; Parker and Andrews, 1986; Odgaard and Bergs, 1988; Furbish, 1988b, c). In particular, flow asymmetry is related to channel curvature according to a spatial convolution. This means that the influence of curvature is cumulative: the flow asymmetry, reflected by cross-channel displacement of the filament of high velocity, starts to develop at the entrance of a bend and increases downstream as far as the channel curvature (the bend) is sustained. Rates of channel migration, measured orthogonally to the centerline, mimic this spatial pattern and reflect increased boundary stresses on the outside bank.

Specific evidence that flow field structure derives from a convolution of channel shape has been presented for the cases of single-thread rivers of moderate size (Howard and Knutson, 1984; Parker and Andrews, 1986; Furbish, 1988a, c), a small, bouldery mountain stream (Furbish, 1985; 1987), and a constant-curvature laboratory channel (Odgaard and Bergs, 1988; also see Furbish, 1988c). The objective of this paper is to demonstrate that the convolution idea is independent of scale, and therefore applies equally to large rivers. This involves recasting the convolution model, as it is presented by Parker and Andrews (1986), into the general form of a stochastic, linear difference equation. Using the spatial

counterpart of Box-Jenkins-style time series analysis, a specific linear form is then estimated from data concerning curvature and thalweg position along the Ohio River; and it is this form that can be compared with the convolution model.

The convolution model has immediate engineering applications that involve predicting where bend erosion will occur, and where navigable channel depths are likely to persist. From a geological viewpoint, the convolution model is novel. It describes a channel evolution that is markedly different from the asymptotically stable behavior suggested by traditional models of meander growth and evolution (e.g. Langbein and Leopold, 1966; Keller, 1975). In particular, a convolution relation between channel migration and curvature precludes the possibility that a steady-state meander geometry exists (Parker and Andrews, 1986; Furbish, 1985; 1988c, d). This leads to implications regarding long-term channel evolution and construction of the fluvial landscape, and arrangement of sediments within it.

FLOW STRUCTURE

The convolution model essentially describes how rapidly the centerline of a curved, single-thread channel migrates based on the strength of the current next to the outside bank. The model therefore emphasizes the importance of outside bank erosion in the migration process, and loosely links this erosion to the increased shear stresses imposed on the outer bank relative to the stresses occuring in a straight channel. It is assumed that these stresses are proportional to the difference between the depth-averaged flow velocity near the bank and the reach-averaged centerline velocity. For the problem considered herein, it is sufficient to note that this velocity difference scales with the flow-field asymmetry, as measured by transverse displacement of the high velocity filament from the channel centerline. The actual relation between filament position and local migration rate is not essential to the development below. So emphasis is placed on the relation between curvature and flow asymmetry, which is reflected by the transverse position of the thalweg along the Ohio River.

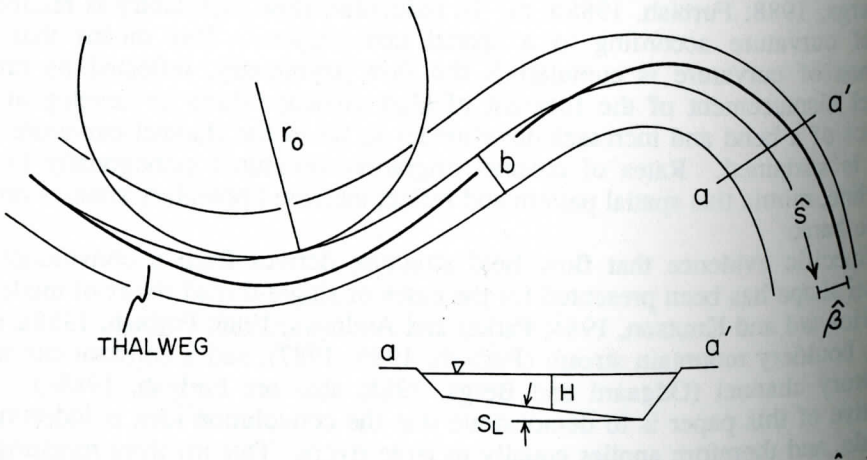

Figure 1. Idealized river channel illustrating centerline arc distance $\hat{s}$; local centerline radius of curvature r_0; channel half-width b; transverse bed slope S_L; centerline depth H; and thalweg displacement $\hat{\beta}$.

The convolution model uses the description of flow in a river bend provided by Engelund (1974). Essential symbolism includes (refer to Figure 1): arc distance along the channel centerline $\hat{s}$; local, centerline radius of curvature r_0; channel half-width b; and transverse bed slope S_L. Define centerline values of depth H, water surface slope I, and vertically averaged streamwise velocity U. Let $\hat{\beta}$ denote the normal distance that the thalweg is displaced from the channel centerline. A scour factor A and a friction factor C_f are defined by

$$A = S_L r_0/H \;\; ; \;\; C_f = gHI/U^2$$

where g is acceleration due to gravity. If H_0, I_0 and U_0 denote values of H, I and U occurring in a straight channel, the problem can be cast in dimensionless form (Parker and Andrews, 1986) by defining the variables

$$s = \hat{s}/H_0 \;\; ; \;\; C^* = b/r_0 \;\; ; \;\; \chi = U/U_0$$

Similarly, a dimensionless value of displacement may be defined by

$$\beta = \hat{\beta}/b$$

This local displacement of the thalweg may be treated as deriving from a convolution of the dimensionless curvature C^*

$$\beta = \int_{-\infty}^{s} f(s - s')\, C^*(s')\, ds' \qquad (1)$$

Equation (1) implies that local thalweg displacement is a weighted aggregate of the entire, upstream curvature series. The impulse response function $f(s)$ is

$$f(s) = D_0[-\chi\delta(s) + C_f(A + 2)\chi^2 \exp(-2\chi C_f s)] \qquad (2)$$

in which D_0 is a dimensionless coefficient set herein to unity. The term in (2) containing the delta function describes a local irrotational influence that tends to keep the filament of high velocity near the inside bank. The term containing C_f describes a cumulative influence whereby the filament of high velocity is driven toward the outside bank. When Equation (2) is multiplied by a dimensionless coefficient of bend erosion (E_0 in Parker and Andrews, 1986), the model predicts a shift of maximum erosion to positions downstream of curvature apexes, a translation of meanders downvalley, and attenuation of short bends (Howard and Knutson, 1984; Parker and Andrews, 1986; Furbish, 1985; 1988c).

The displacement distance β and curvature C^* in Equation (1) can be treated as random variables which, for a long meander train, are symmetrically distributed about zero means. Thus, β and C^* conveniently may be considered as deviations about zero origins. The series of β and C^* further can be treated as discrete, spatial processes: using the notation of Box and Jenkins (1976), Equations (1) and (2) become

$$\beta_s = -kC^*_s + k' \sum_{j=0}^{\infty} \phi^j C^*_{s-j} \qquad (3)$$

where

$$k = D_0\chi$$

$$k' = D_0(A + 2)\chi(1 - \phi)/2$$

$$\phi = \exp(-2\chi C_f \Delta s)$$

The weighting function ϕ^j is independent of the curvature series $\{C^*_s\}$, so (3) can be expressed as a finite autoregressive process (Furbish, 1985; 1988c)

$$\beta_s = \phi\beta_{s-1} + \phi kC^*_{s-1} + (k'-k)C^*_s \qquad (4)$$

Equation (4) implies that the thalweg displacement at site s can be predicted from the displacement at site s-1 upstream if effects of local curvature are taken into account. By replacing D_0 with E_0 in the coefficients k and k', (4) can be used to test for the underlying convolution structure implied by (1). This structure has been confirmed (Furbish, 1988a, c) using data from Hickin and Nanson (1975) concerning curvature and migration for bends of the Beatton River, Canada.

Let z_s denote a random variable, and define the backward shift operator B by the relation $B^m z_s = z_{s-m}$. Again using conventional Box-Jenkins symbolism, (4) has the general form of a stochastic, linear difference equation (Furbish, 1985)

$$\beta_s = \frac{(\omega_0 - \omega_1 B - \ldots - \omega_u B^u)}{(1 - \delta_1 B - \ldots - \delta_v B^v)} C^*_s + N_s$$

$$\beta_s = \delta^{-1}(B)\ \omega(B)C^*_s + N_s \qquad (5)$$

in which the ω's are moving-average coefficients to order u and the δ's are autoregressive coefficients to order v. N_s is noise, assumed independent of the level of C^*, and additive with respect to the influence of C^*. Evidently $u = v = 1$, $\omega_0 = k' - k$, $\omega_1 = -\phi k$ and $\delta_1 = \phi$ in the specific case of (4), giving

$$(1 - \delta_1 B)\beta_s = (\omega_0 - \omega_1 B)C^*_s + N_s \qquad (6)$$

Independent of the linear filter $\delta^{-1}(B)\ \omega(B)$, the curvature series $\{C^*_s\}$ itself can be represented by a difference equation having the form of (5). Such a representation is symbolized herein by

$$C^*_s = \gamma^{-1}(B)\ \varepsilon(B)a_s \qquad (7)$$

where a_s is white noise. This opens the possibility of using the methods of time

series analysis to derive least squares estimates of the parameters in (6), a topic that is examined thoroughly in the classic treatise of Box and Jenkins (1976). While this is an important problem (considered in a different paper), the main task here is to determine whether time series analysis — that is its spatial counterpart — independently retrieves the specific order of difference equation postulated in the model (6). This involves identifying the appropriate "Autoregressive Integrated Moving Average" (ARIMA) transfer function relating thalweg displacement to channel curvature. Identification begins with describing the displacement and curvature series of the Ohio River.

OHIO RIVER

Downstream from Louisville, Kentucky, the Ohio River has two long reaches devoid of major tributaries, islands and engineered structures. These reaches extend approximately from Rock Haven to Cloverport, Kentucky, and coincide with navigation miles 635 to 659, and 663 to 715. The average width of the

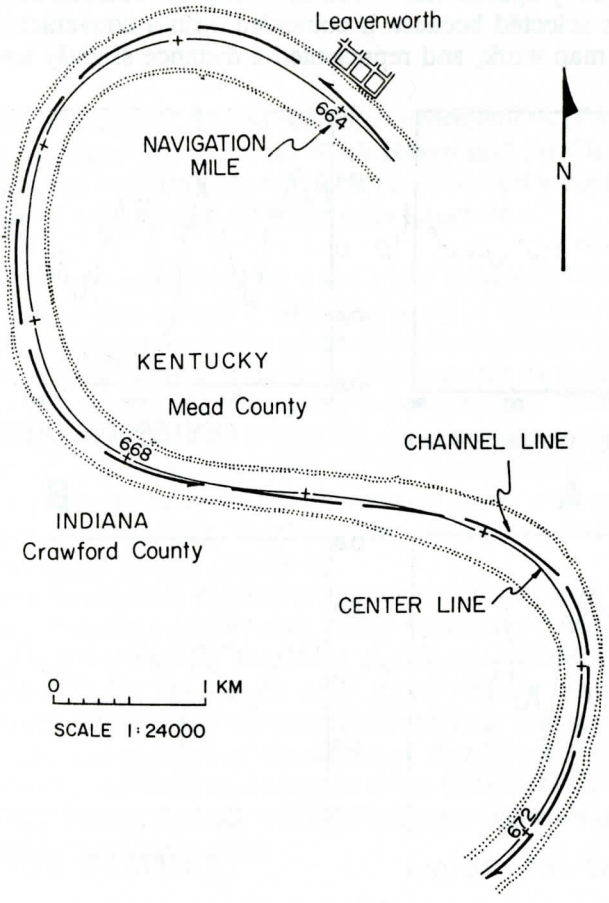

Figure 2. Portion of navigation chart (USACE, 1979) for Ohio River near Leavenworth, Indiana, showing channel line position.

upper "Rock Haven reach" is about 507 m. The average width of the lower "Cloverport reach" is about 516 m. A very good approximation of the thalweg position is provided by the "channel line" — the line within the river marking the contiguously deepest course available for barge and riverboat draft (Figure 2). The channel line periodically is sounded and mapped by the United States Army Corps of Engineers, and documented in navigation charts that are available from Army Engineer District offices (e.g. USACE, 1979).

The channel line is partly maintained by dredging, but this is important more for depth than channel line position. Therefore the channel line reflects the thalweg position as it is maintained normally by transient erosion and deposition. In a curved channel the transverse position of highest specific discharge typically coincides with the thalweg. Inferably the channel line coincides with the filament of high velocity; so displacement of the channel line from the centerline is a reasonable measure of flow-field asymmetry, as asserted in the previous section.

Thalweg displacements and centerline curvatures were estimated at 87 sites along the Rock Haven reach, and at 170 sites along the Cloverport reach (Figure 3). Sites were equally spaced (Δs = 480 m) along the channel centerline. A spacing of 480 m was selected because it coincided with a convenient ruler increment (1 cm) for the map work, and represented a distance slightly less than the average

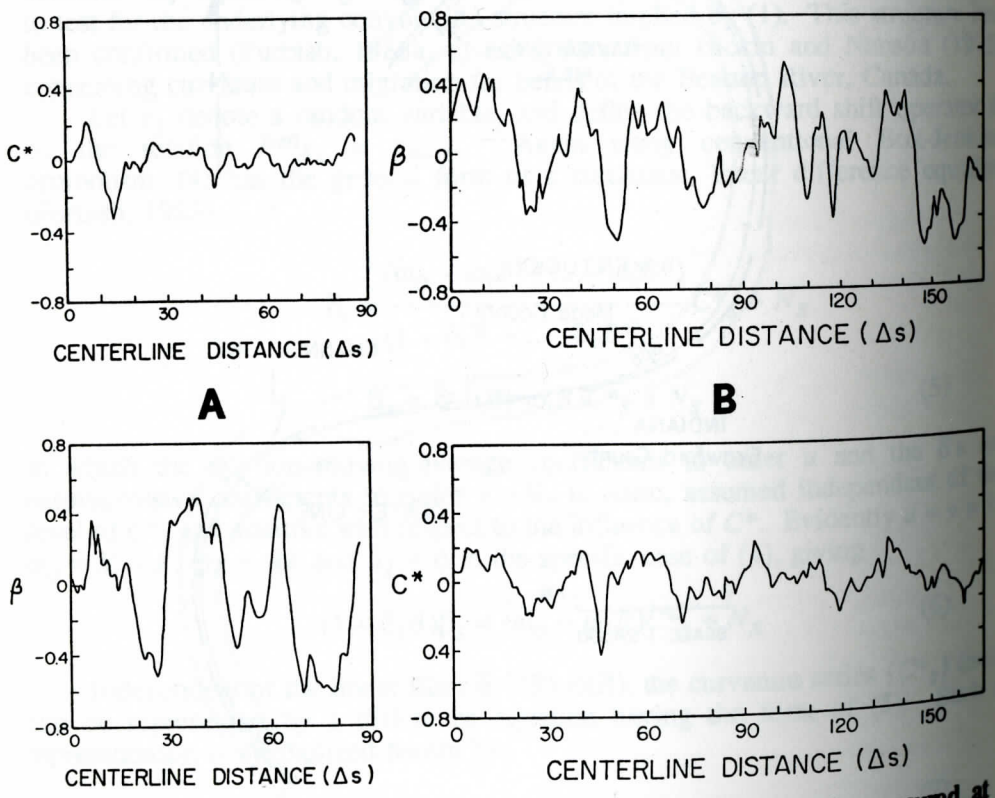

Figure 3. Centerline curvature C^* and thalweg displacement β measured at equispaced sites (Δs = 480 m) along the (a) Rock Haven and (b) Cloverport reaches of the Ohio River.

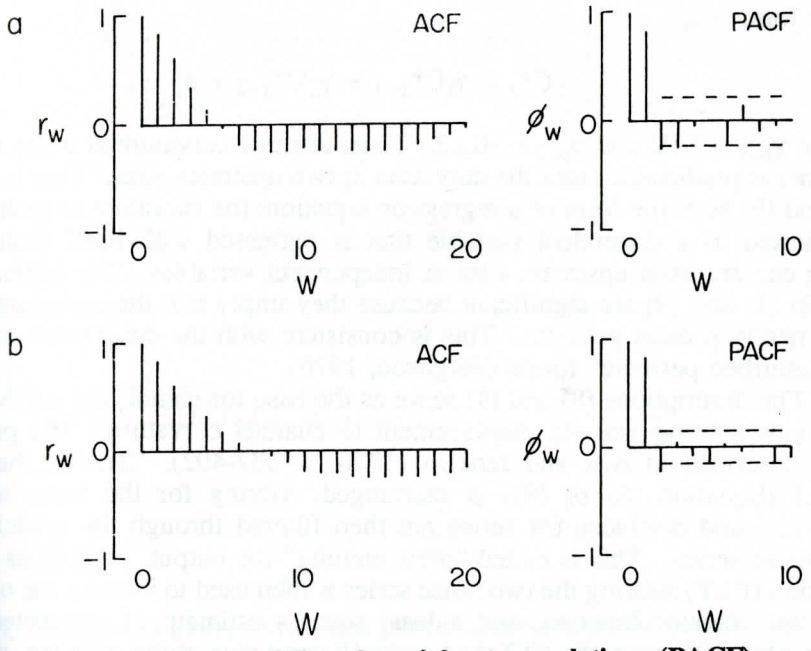

Figure 4. Autocorrelations (ACF) and partial autocorrelations (PACF) over lag *W* for curvature *C measured along the (a) Rock Haven and (b) Cloverport reaches. Dashed horizontal lines with PACF's represent two standard error limits calculated on the assumption of a first-order autoregressive structure.**

channel width. The local curvature C at a site s was estimated using the difference in the map azimuths of chords having endpoints at s-1, s and at s, s+1. A positive curvature is taken as counterclockwise progression in azimuth downstream, and so coincides with "lefthand" bends. Thalweg displacement is made dimensionless using local half-width b since channel width is not constant. The displacement is taken as positive when the thalweg is between the centerline and right bank. The cumulative effect of curvature, described by the summation in (3), is reflected twofold: Relative positions of apexes in the thalweg series tend to mimic those in the curvature series. Moreover, displacement apexes are shifted to positions downstream of curvature apexes (Figure 3).

The curvature series have distinctive autoregressive forms. This is reflected by autocorrelation functions (ACF) that decay slowly with lag, and by partial autocorrelation functions (PACF) that have significant values only at low lags (Figure 4). Each vertical bar of an ACF represents the statistical similarity (correlation) between all observed values separated by the indicated distance (lag). Each bar of a PAFC is a measure of the statistical significance of the correlations described by the ACF. A PACF is analogous to the partial coefficients in multiple regression analysis. A least squares analysis indicates that the Rock Haven series has a third order autoregressive form

$$C^*_s = \gamma_1 C^*_{s-1} + \gamma_3 C^*_{s-3} + a_s \qquad (8)$$

where $\gamma_{s-1} = 1.00$ and $\gamma_{s-3} = -0.26$. The Cloverport series has a second

order form

$$C^*_s = \gamma_1 C^*_{s-1} + \gamma_2 C^*_{s-2} + a_s \qquad (9)$$

where $\gamma_{s-1} = 1.02$ and $\gamma_{s-2} = -0.23$. Thus, channel curvature at a site s along the channel is predictable from the curvature at two upstream sites. That is, Equations (8) and (9) have the form of a regression equation: the curvature at each site s may be viewed as a dependent variable that is regressed with itself (autoregressed) using curvatures at upstream sites as independent variables. The estimated values of γ in (8) and (9) are significant because they imply that the curvature series are very nearly pseudo periodic. This is consistent with the description of meanders as "disturbed periodic" forms (Ferguson, 1976).

The descriptions (8) and (9) serve as the base for identifying ARIMA transfer functions relating thalweg displacement to channel curvature. The procedure is fully described in Box and Jenkins (1976, p. 337-402). Briefly, the curvature model (Equation (8) or (9)) is rearranged, solving for the noise term. The curvature and displacement series are then filtered through the model retrieving two noise series. This is called "prewhitening" the output. The cross correlation function (CCF) relating the two noise series is then used to identify the orders u and v of the transfer function, and a least squares estimate of parameter values is made. In both cases, the CCF had a significant value at the zero lag, a maximum value at the first lag, and then decayed exponentially with higher lags. This CCF form is consistent with the orders $u = v = 1$ (Box and Jenkins, 1976), as postulated in (6). The derived parameter values (Table 1) provide estimates of dimensionless velocity χ, scour factor A and friction factor C_f that are reasonable for large rivers (Parker and Andrews, 1986). This result provides further evidence for the postulated form of (6), although it is not the outcome of a rigorous test.

Table 1. Estimates of transfer function parameters δ_1, ω_0 and ω_1; and dimensionless velocity χ, scour factor A and friction factor C_f for Rock Haven and Cloverport reaches.

	Parameter					
Reach	δ_1	ω_0	ω_1	χ	A	C_f
Rock Haven	0.90	0.23	-0.51	0.57	27	0.0002
Cloverport	0.72	0.15	-0.38	0.53	7	0.0006

An additional result was not anticipated. Equation (6), like (8) and (9), can be rearranged to solve for the noise term. When curvature and displacement series are then filtered through the transfer function, this term consists of the residuals formed by the difference between predicted and observed displacements. This residual series should, in general, consist of uncorrelated noise if the transfer function completely characterizes the relation between curvature and displacement. However, the ACF and PACF for each residual series indicate an

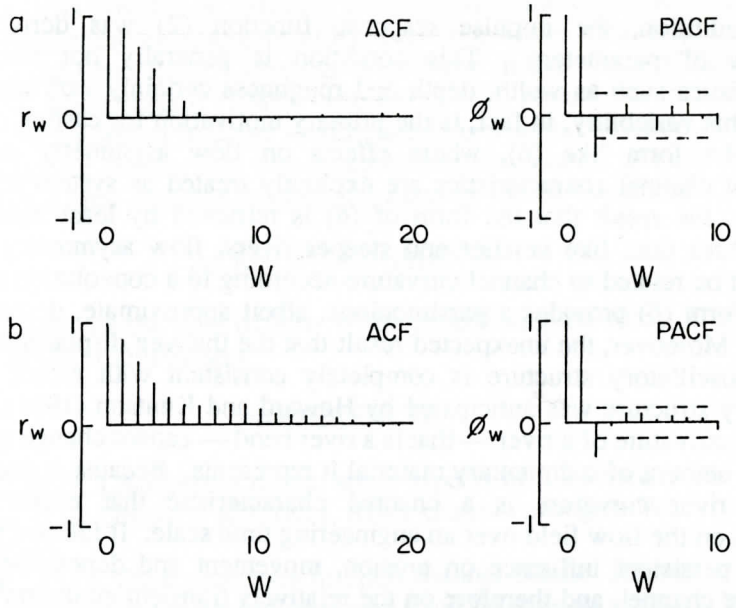

Figure 5. Autocorrelations (ACF) and partial autocorrelations (PACF) over lag W for residuals N_S in Equation (6) calculated for the (a) Rock Haven and (b) Cloverport reaches.

oscillatory structure (Figure 5). Evidently, the form of (6) provides a parsimonious, but inexact, description of the relation between displacement and curvature. In fact, the recent work of Odgaard (1986) and the experiments of Odgaard and Bergs (1988) indicate that the flow asymmetry and cross-channel bed slope in a long bend with constant curvature may have small, but persceptible, damped sinusoidal structures, rather than the simple exponential structure implied by the impulse response function (2). Unfortunately, the data described herein are too crude to rigorously test for a sinusoidal structure.

DISCUSSION

Numerous depth-integrated treatments of the mechanics of flow within curved channels are available. Odgaard and Bergs (1988) compare several models, including that of Engelund (1974), in terms of how well they describe essential features of the flow field by accounting for various acceleration components in the governing equations. Their analyses and experiments indicate clearly that flow field asymmetry responds to channel curvature, and changes in curvature, in a convolution manner. Moreover, this spatial structure is also predicted by the flow model of Odgaard (1986). Thus, abundant theoretical work — in addition to that of Parker and Andrews (1986) and Furbish (1988b, c) — supports a convolution form of relation between flow asymmetry and curvature. However, it remains uncertain whether this convolution structure, as embodied in (1), actually has a simple linear form, or whether it is nonlinear. Parameters in (2) probably are not wholly independent of the coordinate s, and therefore may be colinear with C^* (Furbish, 1988c). This remains an important, open issue.

In addition, the impulse response function (2) was derived assuming constancy of parameters. This condition is generally not true. Channel characteristics such as width, depth and roughness certainly vary along the Ohio River. This variability, in fact, is the primary motivation for casting (1) and (2) in an ARIMA form like (6), where effects on flow asymmetry deriving from inconstant channel characteristics are explicitly treated as system noise. Taking this view, the result that the form of (6) is retrieved by least squares methods demonstrates that, like smaller and steeper rivers, flow asymmetry in the Ohio River can be related to channel curvature according to a convolution relation. The discrete form (6) provides a parsimonious, albeit approximate, description of this relation. Moreover, the unexpected result that the thalweg displacement may have a small oscillatory structure is completely consistent with recent theory. An oscillatory structure was anticipated by Howard and Knutson (1984).

The curvature of a river — that is a river bend — cannot change quickly due to the large amount of sedimentary material it represents. Because it does not change quickly, river curvature is a channel characteristic that exerts a persistent influence on the flow field over an engineering time scale. It follows that curvature exerts a persistent influence on erosion, movement and deposition of sediment within the channel, and therefore on the relatively transient evolution of bed forms that are significantly smaller than bends. Since the thalweg is by definition a feature of the ensemble of bed forms within a river, it is not surprising that a straightforward relation between the thalweg position and curvature can be demonstrated. In effect, Equation (6) formalizes the persistency in thalweg position that should be expected once the influence of curvature on flow structure is known.

On the other hand, maintenance of a thalweg by normal channel flows invariably involves transient changes in bed morphology as relatively small bed forms (dunes, megadunes, bars) move through the channel. This bears on a human issue: Anecdotal evidence for change in river morphology often constitutes no more than a record of local changes associated with normal bedform evolution over a period of 1-2 human generations. Unless related to a catastrophic change in river planform (e.g. a cutoff), the scouring or filling of a favorite fishing or swimming hole — perhaps traumatic to an individual — is not unexpected. This is particularly true in the case of the Ohio River, where the scale of our spatial perception is piddling in comparison to the size of an individual river bend, and our anecdotes span an infinitesimal part of the time required for the meandering process to obliterate a single bend form.

The link between flow asymmetry and bend migration is the item needed for incorporating the convolution idea into predictions of bend erosion and evolution. This pertains to an engineering, as well as geological, time scale. Assuming as described above that the local rate of channel migration scales with flow asymmetry, it follows that the convolution structure described herein underpins meander evolution (Howard and Knutson, 1984; Furbish, 1985, 1988a, c; Parker and Andrews, 1986). The evolution of a meander train can be viewed as the time development of its centerline trace. The curvature $C^*(s)$ thereby undergoes a complementary evolution with the meander train. In effect, the evolution of a meander train is the time-integrated output of a filtering process for which successive states of the evolving curvature series serve as system input (Furbish,

1988c). Thus, it is possible to estimate independently the coefficients in (2) and (6), then calibrate these equations in order to predict where bank erosion is likely to occur along the Ohio River. This has precedence in the works of Howard and Knutson (1984) and Odgaard (1987). Moreover, it is possible to incorporate (6) into a numerical algorithm in order to simulate longer term evolution of the Ohio River, ultimately for comparison with sedimentological records of bend migration. This is one part of my ongoing research concerning fluvial evolution.

ACKNOWLEDGMENTS

I am grateful for the help of Ron White in reducing the data. This paper is dedicated to William D. Pearson.

REFERENCES

Allen, J.R.L., 1977, Changeable rivers: some aspects of their mechanics and sedimentation: *in* Gregory, K.J. (ed.), River channel changes: Wiley, New York, p. 15-45.

Apmann, R.P., 1972, Flow processes in open channel bends: Journal of the Hydraulics Division, American Society of Civil Engineers, v. 98, p. 795-809.

Box, G.E.P., and Jenkins, G.M., 1976, Time series analysis: forecasting and control: Holden-Day, San Francisco, 575 p.

Begin, Z.B., 1981, Stream curvature and bank erosion: a model based on the momentum equation: Journal of Geology, v. 89, p. 497-504.

Engelund, F., 1974, Flow and bed topography in channel bends: Journal of the Hydraulics Division, American Society of Civil Engineers, v. 100, p. 1631-1648.

Ferguson, R.I., 1976, Disturbed periodic model for river meanders: Earth Surface Processes, v. 1, p. 337-347.

Furbish, D.J., 1985, The stochastic structure of a high mountain stream: Ph.D. dissertation, University of Colorado, Boulder, 365 p.

Furbish, D.J., 1987, The influence of roughness on the thalweg position along a bouldery mountain stream in the Colorado Front Range: Geological Society of America, Abstracts with Programs, v. 19, p. 276.

Furbish, D.J., 1988a, A test of recent convolution-integral models describing the migration of river meanders: International Association for Hydraulic Research, Proceedings of the International Conference on Fluvial Hydraulics '88, Budapest, p. 298-303.

Furbish, D.J., 1988b, River-bend curvature and migration: How are they related?: Geology, v. 16, p. 752-755.

Furbish, D.J., 1988c, Spatial autoregressive structure in meander evolution: Water Resources Research. (submitted)

Furbish, D.J., 1988d, The river-meandering process: evidence for nonlinear chaos: Geological Society of America, Abstracts with Programs, v. 20. (in press)

Hickin, E.J., 1974, The development of meanders in natural river channels: American Journal of Science, v. 274, p. 414-442.

Hickin, E.J., and Nanson, G.C., 1975, Character of channel migration on the

Beatton River, northwest British Columbia, Canada: Geological Society of America Bulletin, v. 86, p. 487-494.
Howard, A.D., and Knutson, T.R., 1984, Sufficient conditions for river meandering: a simulation approach: Water Resources Research, v. 20, p. 1659-1667.
Keller, E.A., 1975, Development of alluvial stream channels: a five stage model: Geological Society of America Bulletin, v. 83, p. 1531-1536.
Langbein, W.B., and Leopold, L.B., 1966, River meanders: theory of minimum variance: U.S. Geological Survey Professional Paper, 422H.
Odgaard, A.J., 1986, Meander-flow model, I: Development: Journal of Hydraulic Engineering, v. 112, p. 1117-1136.
Odgaard, A.J., 1987, Streambank erosion along two rivers in Iowa: Water Resources Research, v. 23, p. 1225-1236.
Odgaard, A.J., and Bergs, M.A., 1988, Flow processes in a curved alluvial channel, Water Resources Research, v. 24, p. 45-56.
Parker, G., and Andrews, E.D., 1986, On the time development of meander bends: Journal of Fluid Mechanics, v. 162, p. 139-156.
Parker, G., Panayiotis, P., and Akiyama, J., 1983, Meander bends of high amplitude: Journal of the Hydraulics Division, American Society of Civil Engineers, v. 109, p. 1323-1337.
USACE, 1979, Navigation charts, Ohio River, Cairo, Illinois to Foster, Kentucky: U.S. Army Corps of Engineers, Louisville District, 600 Federal Place, Louisville, Kentucky 40201, 4 sheets, 108 charts.

SEDIMENT CHARACTERISTICS OF SELECTED BEACH RIDGES ALONG FLORIDA'S NORTHEASTERN COAST

MARC E. EICHENHOLTZ — *Department of Geology, University of Florida Gainesvily 11, FL 32611*

E.C. PIRKLE — *Department of Geology, University of Florida Gainesville, FL 32611*

FREDRIC L. PIRKLE — *E. I. Du Pont de Nemours and Company P.O. Box 753, Starke, FL 32091*

ABSTRACT

Principal component analyses of sediments composing beach ridges on modern barrier islands along Florida's northeastern coast reflect the importance of selective sorting, reworking, and winnowing. Reworking and winnowing processes are shown by the behavior of various heavy minerals. The relatively light heavy minerals such as hornblende, epidote, and garnet have an inverse relationship to the heavier ilmenite. Reworking and winnowing are also reflected by the behavior of the total heavy minerals and the very fine sand. These variables exhibit a positive relationship. Heavy minerals are concentrated during reworking and winnowing because of their high specific gravity. The volume of very fine sand increases with reworking and winnowing because finer grains are shielded by slightly coarser particles and, thus, resist entrainment.

Beach ridges on northern Amelia Island contain only about 1 percent heavy minerals. These heavy minerals along with very fine quartz sand load on the fourth component. In contrast, beach ridges on Little Talbot Island contain almost 7 percent heavy minerals. These heavy minerals along with very fine sand load on the first component. The study shows that more than just a mechanism for concentrating heavy minerals is necessary for the accumulation of ore-grade heavy mineral deposits.

INTRODUCTION

This study was undertaken in order to determine sediment characteristics of beach ridges on modern barrier islands along the northeastern Florida coast. One series of ridges investigated is on the northernmost part of Amelia Island (Figures 1 and 2). These Amelia Island ridges occur just south of the St. Marys River. They trend in an essentially east-west direction parallel to the river, then curve southward to follow the direction of the present shoreline (Figure 2). In addition to the Amelia Island ridges, beach ridges along the landward side of the present beach on Little Talbot Island were studied (Figures 1 and 3). These ridges trend in a north-south direction parallel to the present shoreline and were formed in an environment more distant from the influence of a major river. The sediments composing the ridges on both Amelia and Little Talbot islands are predominantly fine quartz sand (Tables 1 and 2).

The sands of the ridges on northern Amelia Island contain an average of 1.07 percent heavy minerals. In contrast, the sands of the ridges on Little Talbot Island

contain an average of 6.9 percent heavy minerals. The principal heavy minerals in these ridge sands are ilmenite, epidote, zircon, kyanite, sillimanite, hornblende, staurolite, rutile, leucoxene, garnet, and tourmaline (Tables 3 and 4).

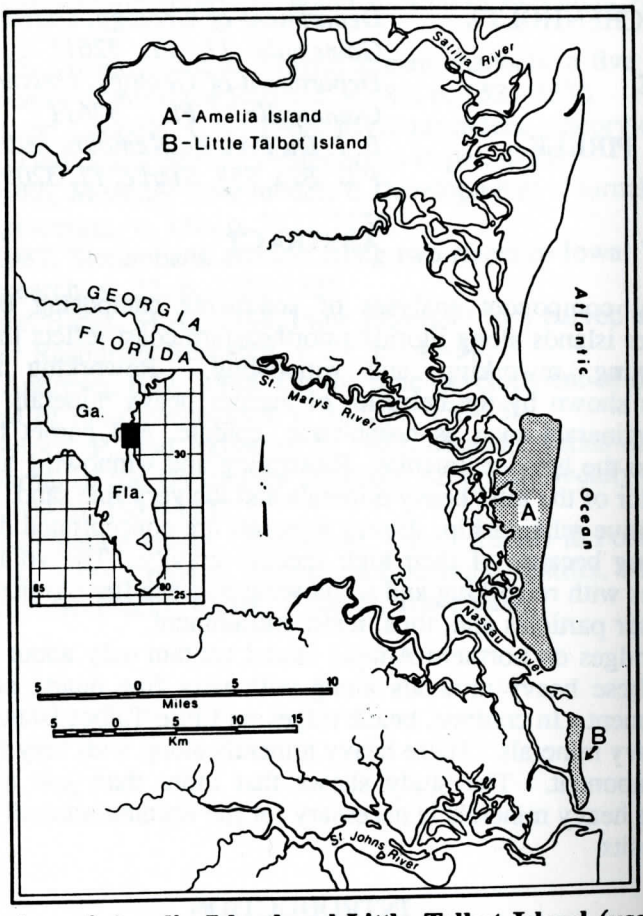

Figure 1. Location of Amelia Island and Little Talbot Island (used through the courtesy of William A. Pirkle).

In carrying out this investigation, the grain-size distribution of quartz sand composing the ridges, the total heavy mineral concentrations in the ridge sands, and the percentages of selected heavy minerals from the sands were examined. Procedures used in the sampling of the sands, in the laboratory analysis of the sediments, and in the sample preparation for petrographic analysis are briefly described in the Appendix. Statistical methods were used to assist in the interpretation of these data.

STATISTICAL ANALYSIS

Multivariate Analysis

Multivariate analysis is a class of statistical tools which may be used to help

Table 1. Mechanical Analyses of Sand from Selected Sites along Amelia Island East-West Ridges. Hole Locations are shown on Figure 2.

Hole Number	Depth of sample in feet	Percent Sand[1] retained								Heavy Minerals in percent
		35 mesh (<1φ)	45 mesh (1-1½φ)	60 mesh (1½-2φ)	80 mesh (2-2½φ)	120 mesh (2½-3φ)	170 mesh (3-3½φ)	230 mesh (3½-4φ)	pan (>4φ)	
1	0-2½	0.0	0.4	6.1	40.8	49.7	3.0	0.0	0.0	.27
	2½-4	0.0	0.2	4.0	36.9	55.2	3.6	0.1	0.0	.43
2	0-2½	0.0	0.2	3.0	36.8	56.0	3.9	0.0	0.0	.15
	2½-5	0.0	0.0	2.1	27.8	64.3	5.7	0.1	0.0	.38
3	0-2½	0.1	0.4	3.4	32.9	58.6	4.5	0.1	0.0	.52
	2½-5	0.0	0.4	3.8	34.6	56.8	4.1	0.2	0.0	1.51
4	0-2½	0.5	0.9	5.1	39.3	51.4	2.7	0.1	0.1	.17
	2½-5	0.1	0.8	6.2	40.4	49.9	2.5	0.0	0.0	.44
	5-7½	0.0	0.4	3.9	35.7	56.9	3.2	0.0	0.0	.47
5	0-2½	0.1	0.8	6.8	37.7	50.6	3.7	0.3	0.0	1.40
	2½-5	0.0	0.5	6.2	44.2	45.1	3.5	0.4	0.0	2.21
6	0-2½	0.0	0.3	4.2	35.8	56.6	3.8	0.2	0.0	.86
	2½-5	0.0	0.3	3.6	36.4	55.8	3.7	0.3	0.0	1.00
7	0-2½	0.5	0.8	6.2	42.6	46.7	3.0	0.2	0.0	.23
	2½-5	0.1	0.4	4.2	39.5	52.3	3.3	0.2	0.0	.34
	5-7½	0.1	0.2	3.4	38.4	53.9	3.9	0.2	0.0	.29
8	0-2½	0.2	0.4	3.6	45.9	47.3	2.5	0.1	0.0	.49
	2½-5	0.1	1.2	6.4	46.5	43.7	2.1	0.1	0.0	.58
	5-7½	0.0	0.7	4.3	42.5	49.3	3.1	0.1	0.0	.84
	7½-9	0.0	0.2	2.6	39.1	54.2	3.9	0.1	0.0	.41
9	0-2½	0.3	1.7	7.1	36.2	51.2	3.3	0.2	0.0	.27
	2½-5	0.1	1.2	5.7	31.4	57.0	4.4	0.1	0.0	.39

[1] Quartz sand and heavy mineral sand.

Table 2. Mechanical Analyses of Sand from Selected Sites along Little Talbot Island North-South Ridges. Hole Locations are shown on Figure 3.

Hole Number	Depth of sample in feet	Percent Sand[1] retained								Heavy Minerals in percent
		35 mesh (<1 ϕ)	45 mesh (1-1½ ϕ)	60 mesh (1½-2 ϕ)	80 mesh (2-2½ϕ)	120 mesh (2½-3ϕ)	170 mesh (3-3½ϕ)	230 mesh (3½-4ϕ)	pan (>4ϕ)	
1	0-2½	0.0	0.0	0.4	16.8	65.9	13.6	3.2	0.1	9.89
	2½-5	0.0	0.1	1.4	21.3	63.5	11.3	2.2	0.1	6.73
2	0-2½	0.0	0.1	0.8	20.9	64.5	11.4	2.1	0.1	7.70
	2½-5	0.0	0.0	0.5	22.1	63.7	10.6	2.8	0.1	11.50
3	0-2½	0.0	0.1	0.9	23.5	63.9	9.9	1.7	0.0	6.27
	2½-5	0.0	0.2	0.9	23.9	64.6	8.8	1.8	0.0	5.63
4	0-2½	0.0	0.2	1.7	30.6	58.1	7.8	1.4	0.1	4.02
	2½-5	0.2	0.4	2.0	32.1	56.3	7.6	1.3	0.1	3.84
5	0-2½	0.0	0.2	3.1	43.5	45.8	6.1	1.1	0.1	3.06
	2½-5	0.0	0.4	3.4	33.7	54.3	6.9	1.1	0.2	3.12
6	0-2½	0.0	0.1	1.0	26.5	54.1	13.4	4.6	0.3	16.4
	2½-5	0.0	0.6	2.7	20.0	57.4	14.4	4.6	0.3	13.0
7	0-2½	0.1	0.4	3.4	36.2	48.1	9.0	2.5	0.2	7.96
	2½-5	0.0	1.2	2.4	21.1	59.7	12.5	3.0	0.2	8.87
8	0-2½	0.1	0.3	2.3	31.6	52.6	10.3	2.6	0.2	9.36
	2½-5	0.5	1.4	4.4	29.1	50.0	11.0	3.2	0.3	9.90
9	0-2½	0.2	0.6	3.5	36.5	48.7	8.6	1.8	0.1	6.62
	2½-5	0.0	0.1	1.4	24.3	58.2	13.1	2.8	0.0	11.33

[1]Quartz sand and heavy mineral sand.

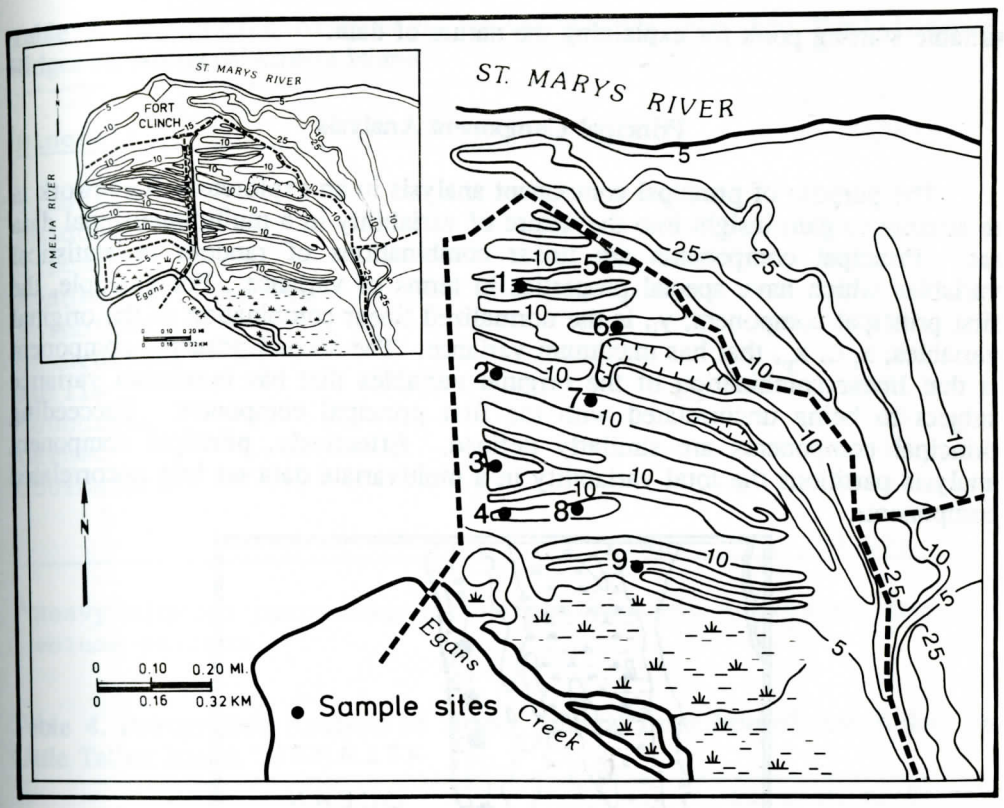

Figure 2. East-west trending ridges on northern Amelia Island. Analyses of samples from selected holes (black circles) are given in Table 1. Contour lines are in feet above mean sea level.

in understanding the interactions of variables. Common techniques of multivariate data analysis include principal component analysis, factor analysis, discriminate function analysis, and cluster analysis.

Often an investigator may not know in advance the structural features of data which will be most susceptible to meaningful interpretation. This is especially true for multivariate data which, partly because of the interrelated character of the variables, is inherently complex. In many instances, therefore, it is best not to leave the multivariate analysis of data to a rigidly prespecified method which must be based upon specific assumptions (either explicit or implicit). In these cases the techniques needed to study the multivariate data are exploratory techniques. These techniques produce a model or explanation of features of the data.

In contrast, confirmatory analyses may be performed to test specific hypotheses. Such analyses are based on a model not derived from the data to be analyzed. Like many other forms of statistical inference, a confirmatory analysis is focused on the estimation of parameters and on tests for hypothetical values of parameters.

The principal statistical application used in this study is exploratory in nature with principal component analysis being utilized to help in the interpretation of the data. Principal component analysis is straightforward in application and provides a

suitable starting point for explaining the nature of data.

Principal Component Analysis

The purpose of principal component analysis in an exploratory framework is to attempt to gain insight into the nature of variability in a multidimensional data set. Principal components are linear combinations of random or statistical variables which have special properties in terms of variance. For example, the first principal component, y_i, is the normalized linear combination of the original variables, x_i ... x_p, that has maximum variance. The second principal component is that linear combination of the original variables that has maximum variance subject to being uncorrelated with the first principal component. Succeeding principal components are similarly defined. Effectively, principal component analysis partitions the total variability in a multivariate data set into uncorrelated components.

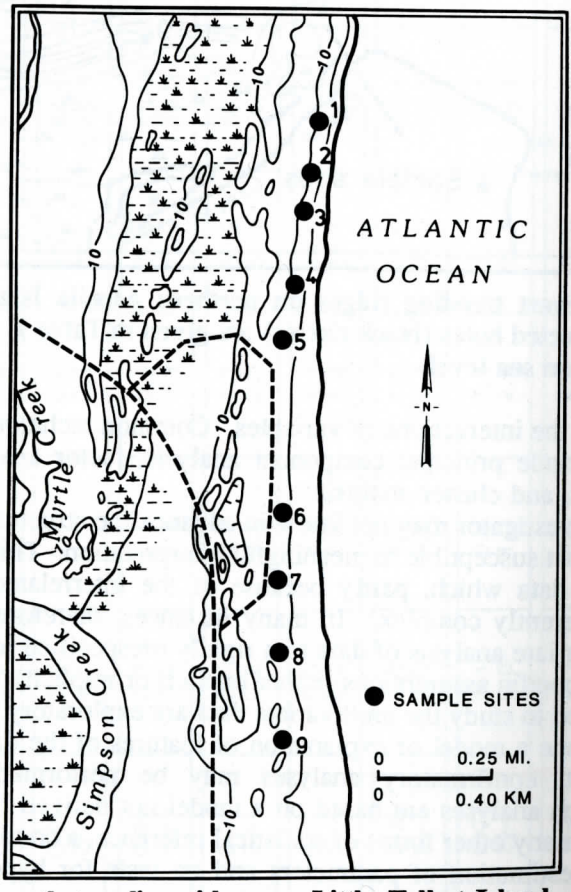

Figure 3. North-south trending ridges on Little Talbot Island. Samples for this study were taken along ridges bordering the landward side of the present beach. Analyses of samples from selected holes (marked by black circles) are given in Table 2. Contour lines are in feet above mean sea level.

Table 3. Petrographic Analysis of Heavy Minerals from East-West Trending Ridges on Northern Amelia Island

Minerals	Percent of Total Heavy Minerals[1]
Ilmenite	50.28%
Epidote	22.31%
Zircon	6.61%
Kyanite/Sillimanite	6.02%
Hornblende	4.13%
Staurolite	3.18%
Rutile	2.63%
Leucoxene	1.91%
Garnet	1.48%
Tourmaline	1.45%
TOTAL	100.00%

[1]Heavy mineral percentage is weight percent converted from volume percent.

Table 4. Petrographic Analysis of Heavy Mineral from North-South Ridges on Little Talbot Island.

Minerals	Percent of Total Heavy Minerals[1]
Ilmenite	53.20%
Zircon	14.68%
Epidote	12.32%
Kyanite/Sillimanite	5.66%
Rutile	4.92%
Staurolite	4.13%
Garnet	1.70%
Leucoxene	1.37%
Hornblende	1.29%
Tourmaline	0.52%
TOTAL	100.00%

[1]Heavy mineral percentage is weight percent converted from volume percent.

In many exploratory studies the number of variables under consideration is too large for assimilation. A way of reducing dimensionality is to keep only those principal components that account for a suitably large fraction of the total variance and to ignore the rest. Commonly a very small number of components can be used

to summarize the original data.

There are two modes which may be used for principal component analyses. One is the Q-mode, which can be performed to inspect the interrelationships among samples. This mode provides a descriptive technique capable of giving equal and simultaneous consideration to a number of sediment properties. Such an analysis is useful in determining which sediments have like properties and can lead to the classification of samples in relation to "end member" components (Klovan, 1966).

The second mode, the R-mode, may be used to compare interrelationships among variables. Relationships between variables based on all samples are compared. In this mode, the matrix of observations is simplified by determining the minimum number of components needed to account for most of the variation in the original set of test variables. This mode is used to group the measured values into components (similar associations). Variables which load on the same component are assumed to have been affected by a similar process or processes. The interpretation consists of specifying the mechanism responsible for the components (Allen and others, 1972). "Identification of the particular process accounting for the variation of a set of variables is the researcher's prerogative" (Ondrick, 1968, p.127).

If a variable is affected by only one process, the "loading" of that variable with respect to the component is given a value of 1.00. If the component represents a process that has no effect on the variable, the "loading" is zero. Usually, any one variable will be affected by a number of processes with one process being dominant.

Ondrick (1968) states:

> The R-mode principal component analysis can help the investigator studying sedimentary rocks and sedimentary features to answer at least three questions: (1) How many and which of the variables are affected by a similar process or processes? (2) How many processes are of major importance in the formation of a given "rock or sedimentary body?" (3) Which process or processes are most instrumental in the formation of a given "rock or sedimentary body?"

These questions are fundamental to this study where "beach ridge" may be substituted for the terms "rock or sedimentary body."

In this investigation the computer program BMDP4M (Dixon, 1981, revised 1983) was utilized in performing principal component analyses (R-mode) on variables derived from analyzing the sediment samples collected from the beach ridges. Because the loadings of some variables tended to split across several factors, a Varimax rotation was performed. The actual number of components retained for interpretation was based on the criterion proposed by Kaiser (1960). He states that only those components with eigenvalues greater than one should be retained.

VARIABLES ANALYZED

In performing the principal component analyses on the beach ridge sediments

the particle sizes in weight percent were analyzed because they may reflect sediment source or modes of sediment transport, and, indirectly, environments of sediment deposition. The total heavy mineral content in weight percent was considered because such data may reflect source area or reworking and sorting. The percent of certain heavy minerals, namely ilmenite, leucoxene, epidote, garnet, and hornblende were chosen for close examination because these heavy minerals may be useful indicators of reworking, winnowing, and post-depositional weathering. These five heavy minerals were extracted from the very fine sand fraction (3 phi to 4 phi or 0.125 mm to 0.062 mm).

INTERPRETATION OF ANALYSES

An examination of the principal component analysis performed on the samples collected from the Amelia Island ridges shows that four component groupings explain 78 percent of the variation (Table 5). The smaller sand particles, except for the 3 1/2 phi to 4 phi size fraction, load on component 1, and the larger size particles load on component 3. These are size components. The heavy minerals, ilmenite, hornblende, and epidote load on component 2. This, therefore, is a compositional component. The total heavy minerals load with the 3 1/2 phi to 4 phi size sand and with leucoxene on component 4. The leucoxene, however, is not well explained (low communality).

Table 5. Northern Amelia Island – East-West Ridges. Diagonalized simplified Components. Sample size n = 74.

	Principal Components				
Component Property	Component 1	Component 2	Component 3	Component 4	Communality
2 to 2½ ϕ	xxx				0.9052
3 to 3½ ϕ	+++				0.9030
2½ to 3 ϕ	+++				0.9346
Ilmenite		xxx			0.8597
Hornblende		+++			0.8424
Epidote		++			0.6993
Garnet					0.3690
1 to 1½ ϕ			+++		0.8513
<1ϕ			++		0.6546
1½ to 2ϕ			++		0.8507
Heavy Minerals				++	0.8659
3½ to 4ϕ				++	0.8849
Leucoxene				xx	0.5409
Eigenvalue	2.946	2.822	2.475	1.919	
Cumulative Proportion of Total Variance	0.2266	0.4437	0.6340	0.7816	

Explanation

	Positive	Negative
>0.80	+++	xxx
0.60-0.80	++	xx
≤0.60		

$n = 74$, d.f. = 72, $r_{01,72} = 0.3017$, $2r_{01,72} = 0.60$

Table 6. Little Talbot Island – North-South Trending Ridges. Diagonalized simplified components. Sample size n = 74.

Component Property	Principal Components: Component 1	Component 2	Component 3	Component 4	Communality
3½ to 4ϕ	+++				0.9381
Heavy Minerals	+++				0.8594
3 to 3½ϕ	++				0.8039
>4ϕ	++				0.6146
Hornblende	xx				0.6945
2½ to 3ϕ		xxx			0.8937
2 to 2½ϕ		+++			0.8664
1½ to 2ϕ		++			0.7847
Ilmenite			+++		0.8129
Epidote			xxx		0.7881
<1ϕ				++	0.5078
Leucoxene				++	0.4900
1 to 1½ϕ				++	0.6633
Garnet					0.2730
Eigenvalue	3.184	3.014	2.134	1.658	
Cumulative Proportion of Total Variance	0.2274	0.4427	0.5951	0.7136	

Explanation

	Positive	Negative
>0.80	+++	xxx
0.60-0.80	++	xx
≤0.60		

$n = 74$, d.f. $= 72$, $r_{01,72} = 0.3017$, $2r_{01,72} = 0.60$

Four component groupings explain 71 percent of the variance for the ridge sediments of Little Talbot Island (Table 6). The very fine sand, the pan fraction (>4 phi), the total heavy minerals, and hornblende load on component 1. Intermediate size sands load on component 2, and coarser sands load on component 4. Ilmenite and epidote load on component 3.

The results of sorting, reworking, and winnowing by wave and wind action are interpreted to be dominant features of the principal component analyses. To illustrate, selective sorting or reworking is reflected in the behavior of various heavy minerals. In the case of the Amelia Island ridges (Table 5, component 2), the relatively light hornblende (specific gravity of 3.0 to 3.4) and epidote (specific gravity of 3.3 to 3.6) show an inverse relationship to the heavier ilmenite (specific gravity of 4.6 to 4.8). For the ridge sediments of Little Talbot Island (Table 6, component 3), the lighter epidote also shows an inverse relationship to the heavier ilmenite. Furthermore, component 1 of the Little Talbot Island analysis shows that as the total heavy mineral content increases, the relatively light hornblende decreases. The behavior of the heavy minerals with regard to specific gravity is a reflection of reworking and winnowing, processes to which beach ridge sediments are continually subjected as beach ridges develop.

Another strong relationship reflecting reworking and winnowing is shown by the correlation of the total heavy minerals with very fine sands (component 4 for the

ridges on northern Amelia Island, Table 5 and component 1 for the ridge sediments from Little Talbot Island, Table 6). As beach ridge sediments accumulate they are subject to reworking and winnowing by waves and winds. Very fine sands are shielded by slightly coarser particles and thus tend to resist entrainment (Komar, 1987). Therefore, reworking or winnowing of accumulating beach ridge sands may result in an increase in the percentage of heavy minerals with an accompanying increase in the percentage of the very fine sand fraction, relationships shown by the principal component analyses.

It should be noted that the total heavy minerals and very fine sands load on different components for the various ridges. In the case of the ridges on northern Amelia Island the heavy minerals average only 1.07 percent and load with very fine sand (3 1/2 phi to 4 phi) on component 4. For the ridge sediments on Little Talbot Island, the heavy minerals average 6.9 percent and load with the very fine sands (3 phi to 4 phi) on component 1.

COMMENTS AND CONCLUSIONS

In this study the statistical patterns of sediments composing beach ridges formed in different environments were examined. Beach ridges studied on northern Amelia Island developed downdrift from the site where a major river, the St. Marys River, enters the ocean. The ridge sediments studied on Little Talbot Island were collected from ridges along the landward side of the present beach, more distant from the influence of a major river. Furthermore, the sands of the ridges on northern Amelia Island contain only small amounts of heavy minerals, averaging about 1 percent. In contrast, the beach ridge sands from Little Talbot Island are "ore-grade" sands, averaging almost 7 percent heavy minerals. Regardless of the differences in heavy mineral concentrations, the dominant features revealed by the principal component analyses reflect selective sorting, reworking, and winnowing. These are dominant processes to which beach ridge sediments are subjected as beach ridges develop.

A mechanism for concentrating heavy minerals exists at Little Talbot Island and manifests itself on the first component (Table 6). The concentrating process was much less effective in concentrating heavy minerals in the case of the Amelia Island ridges and is expressed on component 4 (Table 5). This study shows that a mechanism for concentrating heavy minerals is not in and of itself sufficient to create a heavy mineral deposit of economic value. In addition to the need for a concentrating mechanism, a source of heavy minerals and a favorable environment for the concentration of the heavy minerals must exist.

The positive relationship between the total heavy minerals and very fine sands as shown by the principal component analyses reflects reworking and winnowing of the sands during extended periods of time. If the heavy minerals had been concentrated by special processes not active throughout most of the time of deposition of the sediments (as would be the case for some storm deposits), the heavies, very likely, would have loaded on a component by themselves. A number of examples are known where heavy minerals of storm accumulations load by themselves on a separate component. Statistical patterns, therefore, do reflect important aspects of the environment in which sediments accumulate.

ACKNOWLEDGMENTS

The authors extend their sincere appreciation to the Florida Department of Natural Resources, Division of Parks and Recreation for permitting the study of beach ridges in Little Talbot Island State Park and in Fort Clinch State Park. Without the cooperation of that organization the study would not have been possible. Also, sincere thanks are extended to E. A. Mallard for his help in collecting samples. The writers are very grateful to E. I. Du Pont de Nemours and Company for permitting analyses to be run in their laboratories. Special thanks are extended to N. W. Stouffer of Du Pont for providing a working environment that was pleasant and stimulating. The manuscript has benefited greatly from reviews by George M. Griffin, Robert C. Lindquist, Roderick W. Tillman, and John G. Reynolds. Thomas R. Bement of the statistics group in the Analytic and Assessment Division of the Los Alamos National Laboratory kindly reviewed the statistical portion of the investigation. Gratitude is expressed to Patti Crawford and Sylvia Atwell for typing the report and aiding in the preparation of tables and figures. The study formed the basis for a thesis submitted to the Department of Geology, University of Florida, in partial fulfillment of the requirement for the M.S. degree.

REFERENCES

Allen, G. P., Castaing, P., and Klingebiel, A., 1972, Distinction of elementary sand populations in the Gironde estuary (France) by R-mode factor analysis of grain size data: Sedimentology, v. 19, p. 21-35.

Dixon, W. J., 1981, BMDP statistical software (revised 1983): Univ. Calif. Press, Los Angeles, p. 480-499.

Eichenholtz, M. E., 1986, Sediment characteristics of selected beach ridges along Florida's northeastern coast: M.S. thesis, Univ. Florida, Gainesville, FL.

Gy, P. M., 1982, Sampling of particulate materials theory and practice, *in* Developments in geomathematics 4: Elsevier Scientific Publishing Co., New York, p. 294-297.

Kaiser, H. F., 1960, The application of electronic computers in factor analyses: Educational and Psychological Measurements, v. 20, p. 141-151.

Klovan, J. E., 1966, The use of factor analysis in determining depositional environments from grain-size distributions: Jour. Sed. Pet., v. 30, p. 115-125.

Komar, P. D., 1987, Selective grain entrainment by a current from a bed of mixed sizes: a reanalysis: Jour. Sed. Pet., v. 57, p. 203-211.

Ondrick, C. W., 1968, Petrography and geochemistry of the Rensselaer graywacke, Troy, New York: Ph. D. dissertation, The Pennsylvania State Univ., University Park, Pa.

APPENDIX

Sampling Methods

Hand-auger samples were collected from 30 holes drilled on Amelia Island

and from 37 holes drilled on Little Talbot Island during the months of February through June, 1985 (Eichenholtz, 1986). From these holes a total of 148 samples were extracted — 74 from Amelia Island and 74 from Little Talbot Island. Nearly all samples were composites of 2 1/2-foot intervals. A few samples were 1 1/2-foot composites. No samples were collected deeper than the base of the sand ridges, and no holes were drilled near man-made structures.

Sample sites were selected so as to best represent each study area. On Amelia Island samples were collected along three north-south traverses through the east-west trending ridges. Samples from Little Talbot Island were collected from holes evenly spaced along the north-south trending ridges bordering the landward side of the present beach.

Laboratory Procedures

All samples were dried at 125-150° C until virtually no moisture remained. Then, each sample was subsampled using a riffle splitter (Jones splitter) into two 100-150 gram splits. The procedures described by Gy (1982) were followed. The "alternation rule" was observed, and the bucket retained was selected by Gy's technical sample method. One split was weighed and placed in a separatory funnel along with acetylene tetrabromide (a liquid with a specific gravity of 2.93). The sample was then stirred and the heavy minerals allowed to settle for 10 minutes. Once at the bottom, the heavy minerals were drained onto filter paper. The sample was again stirred and the heavy minerals again drained. After washing with denatured alcohol (Tecsol) and drying, the heavies were weighed, and the weight percent was calculated for each sample. Finally, the dried heavy minerals were placed in a sonic sifter for 5 minutes with the -120 to +230 mesh-size heavy minerals (3 phi to 4 phi) being removed for petrographic analysis.

The second split from the raw samples was placed in a sieve nest containing 35 mesh (>0.50 mm), 45 mesh (0.35 to 0.50 mm), 60 mesh (0.25 to 0.35 mm), 80 mesh (0.177 to 0.25 mm), 120 mesh (0.125 to 0.177 mm), 170 mesh (0.088 to 0.125 mm), 230 mesh (0.062 to 0.088 mm) screens and a pan (<0.062 mm). The nest was shaken in a Ro-Tap for 20 minutes, and the material retained on each screen was weighed. These measured values were then used to calculate the weight percent for each screen size.

Sample Preparation for Petrographic Analysis

For each sample, a 1,000 to 2,000 grain split of the 3 phi to 4 phi heavy minerals was extracted. Here again, the procedures for subsampling described by Gy (1982) were followed. Next, these heavy mineral grains were immersed in bromonapthalene (index of refraction 1.65) on a clean glass slide. A cover glass was placed over the sample and gently given a circular motion with a clean pencil eraser so as to distribute the grains and avoid overlap. The slide was then ready for counting.

For this study, 300 to 500 heavy mineral grains were counted from the -120 to +230 mesh-size fraction (3 phi to 4 phi). Ilmenite, leucoxene, epidote, garnet, and hornblende were counted individually. All other grain types were grouped into one category and labeled as "others."

PETROLOGY OF SOME LOWER ORDOVICIAN-SILURIAN SEDIMENTARY STRATA FROM THE SOUTHEAST GEORGIA EMBAYMENT, U.S. OUTER CONTINENTAL SHELF

LAWRENCE J. POPPE
WILLIAM P. DILLON

U.S. Geological Survey
Woods Hole, MA 02543

ABSTRACT

The Transco 1005-1 well penetrated 879 m of Silurian and Lower Ordovician sedimentary and metasedimentary rocks. The Silurian section (2,667 to 3,018 m) is composed primarily of black to dark-gray, carbonaceous, fissile shales interbedded with quartz wackes, siltstones, quartzarenites, and dolostones. The shales contain abundant illite/mica and smaller amounts of kaolinite, angular silt-sized quartz and feldspar, pyrite, chlorite, siderite, and calcite. The carbonate rocks contain a similar mineral suite suspended in nonporous anhedral dolomite. The Ordovician section (3,018 to 3,546 m) is composed largely of medium- to fine-grained quartzarenites interlayered with and overlain by quartz wackes, siltstones, and dark-gray shales. The quartzarenites are typically white, mature to submature, and tightly cemented by quartz overgrowths and various amounts of chert and chalcedony; intergrain contacts are often pressure-welded. Some interstitial illite/mica, kaolinite, and chlorite (<10% by volume) are present, but these minerals are partially authigenic. The presence of polycrystalline and semicomposite quartz grains and metamorphic rock fragments indicates a metamorphic component in the provenance. Rounding of the heavy mineral resistates suggests sustained reworking. Diabase intrusions of presumed Triassic or Jurassic age, which were penetrated in two intervals (3,001 to 3,008 m and 3,382 to 3,391 m), exhibit primarily intergranular to subophitic textures. They are composed mainly of labradorite, partially altered pyroxenes, and smaller amounts of magnetite, chlorite, smectites, hornblende, biotite, calcite, epidote, and antigorite. These Paleozoic strata dip to the southeast, occur in a half-graben separated from the overlying nonmarine Lower Cretaceous deposits by an angular unconformity, and suggest a general upward progression from neritic or littoral sands to lower energy shelf-mud and lagoonal facies. This sequence is lithologically similar to the Paleozoic Suwannee Basin strata beneath Florida that were deposited on the African-South American Iapetus continental margin.

INTRODUCTION

The Transco 1005-1 well, located about 108 km off the Georgia coast (Figure 1), was drilled to 3546 m in the Southeast Georgia Embayment, an eastward-plunging basin recessed into the continental shelf between the Carolina and Florida platforms. The Transco 1005-1 well, the Continental Offshore Stratigraphic Test (COST) GE-1 well, and more than 60 wells drilled in

southeastern Alabama, southern Georgia, and northern Florida have penetrated Lower Paleozoic sandstones and shales beneath the Mesozoic, postrift regional unconformity. The Lower Paleozoic deposits encountered by drilling range in age from Early Ordovician to Middle Devonian, based on sparse fossil evidence. Unfortunately, owing to rotation of the down-dropped blocks during normal faulting and to erosion at the postrift unconformity, no single well has penetrated the entire Lower Paleozoic section.

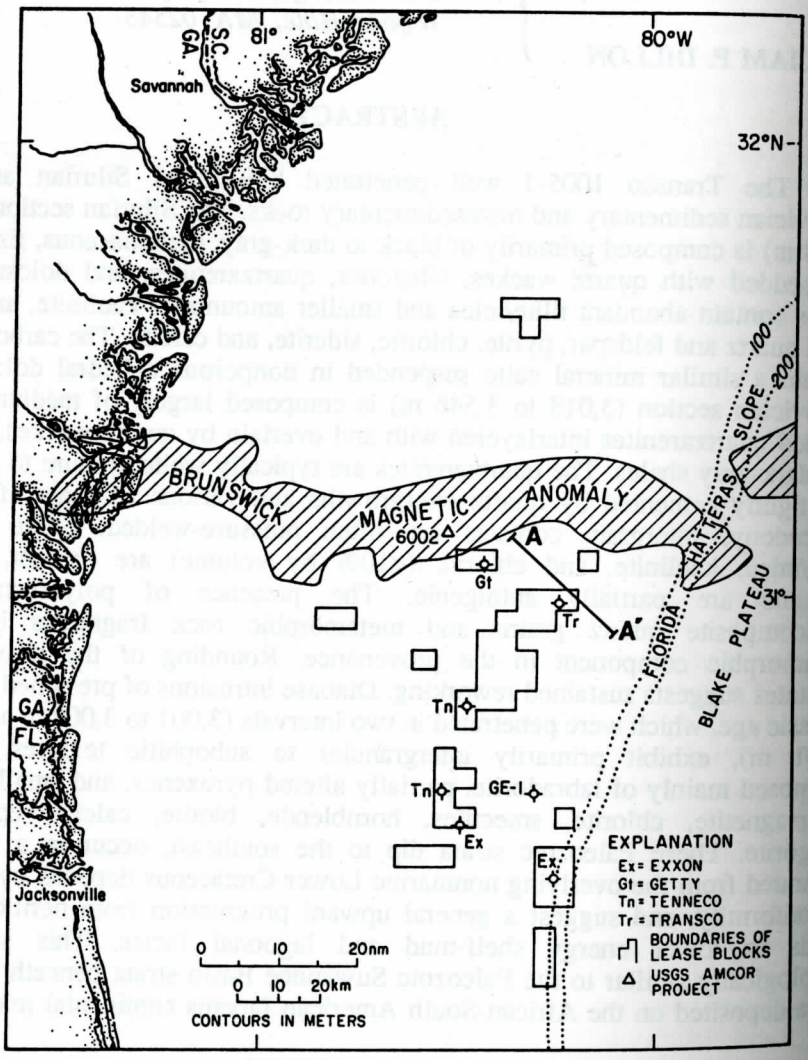

Figure 1. Map showing the location of wells drilled in the Southeast Georgia Embayment, South-Atlantic Outer Continental Shelf. The approximate location of the seismic profile trackline, lease block boundaries, drilling results, and Brunswick Magnetic Anomaly are also plotted on the map.

Although the existence of the onshore Lower Paleozoic sedimentary and very low grade metamorphic rocks has been known for many years (Gunter, 1928;

Applin, 1951), their presence beneath the southeastern U.S. Outer Continental Shelf was not confirmed until exploratory drilling for hydrocarbons occurred during 1977-1979. Seven wells were drilled in the Southeast Georgia Embayment during this period, two of which penetrated Paleozoic strata: the Transco 1005-1 well and the COST GE-1 borehole, which encountered 669 m of argillites, slatey shales, and metaquartzites that were radiometrically dated as Middle Devonian (Scholle, 1979).

The Paleozoic strata penetrated beneath the Coastal Plain sediments of the southeastern U.S. (Carrol, 1963; Cramer, 1971; Neathery and Thomas, 1975; and Pojeta and others, 1976) compare well with descriptions of the Lower Paleozoic sections encountered in the Taoudeni, Senegal, and Bove Basins of West Africa (Sougy, 1962; Dillon and Sougy,1974; and Petters, 1979) and in the Amazon and Parana Basins of Brazil (Soares and others, 1978). The lithological and paleontological similarities between these sections suggest that the pre-Mesozoic sedimentary rocks were deposited on the African-South American Iapetus continental margin and, therefore, represent part of a disjunct fragment of Gondwana that was sutured to the North American craton during the Late Paleozoic Alleghenian Orogeny (Smith, 1982; Chowns and Williams, 1983; Opdyke and others, 1987; Dallmeyer, 1987; and Klitgord and Schouten, 1987). Data from the Consortium for Continental Reflection Profiling (COCORP) has shown that this suture coincides approximately with the Brunswick Magnetic Anomaly (Nelson and others, 1985). Because the Lower Paleozoic deposits of this exotic terrane were located reasonably far to the south and east of the west-trending suture formed in this area during the African-North American continental collision (Cook and Oliver, 1981), they were not subjected to extensive compressional stress and the strata remained relatively unmetamorphosed.

Development of the present continental margin off the southeastern U.S. began with Triassic rifting and stretching of the continental block as Africa, South America, and North America began to move apart (Dillon and Popenoe, 1988; Klitgord and others, 1988). The initial phase of rifting, which was not limited to the earlier suture zone, was characterized by widespread normal faulting resulting in the formation of grabens and half-grabens. Many of the Early Mesozoic rift basins have been identified on land, both exposed and buried beneath coastal plain sediments, and offshore beneath the Atlantic continental margin (Hutchinson, 1986). These basins not only controlled the synrift sedimentation, but, in the case of the basins that now underlie the southeastern United States, protected some of the Paleozoic sedimentary section from erosion.

This paper describes the lithology, x-ray mineralogy, and petrography of the Lower Paleozoic deposits in the Transco 1005-1 well. Their composition is examined to compare them to the stratigraphically equivalent sedimentary rocks beneath the coastal plain sediments and sedimentary rocks of the southeastern U.S., to determine their depositional and diagenetic history, and to refine earlier interpretations of the sedimentary and environmental conditions prevalent in this portion of the Iapetus Ocean.

PROCEDURES

Rotary drill cuttings, in conjunction with available electric logs and sidewall

core descriptions, were used to determine the lithological variations within the well. Cuttings representing distinct lithologies were manually separated from splits of each sample, washed by sonification, crushed, and x-rayed as randomly oriented powders. The clay fraction from each sample was separated by centrifuge and was mounted on a silver filter as an oriented aggregate. Each oriented clay mount was subjected to four treatments to determine which clay minerals were present: air-drying, glycolation with ethylene glycol, heating to 400° C, and heating to 550° C. The samples were x-rayed after each treatment. The data from the oriented and randomly oriented mounts were combined and semiquantitative estimates of the minerals present were made by comparing the sample diffraction peak intensities with the intensities recorded from a collection of standards. Relative percentages of the clay minerals were estimated by a method described by Biscaye (1965). These semiquantitative estimates are generally considered to be accurate to within 10% of their actual values; however, values of components present in smaller amounts (<10%) may have considerably greater error. Splits were taken from twenty of the samples and mounted as thin sections.

All depth references are based on depth below the Kelly Bushing (RKB); which is 31 m above mean sea level and 71.3 m above the sea bottom.

LITHOLOGY AND STRATIGRAPHY

The Transco 1005-1 well encountered rocks formed in environments ranging from terrestrial to upper bathyl (Figure 2); no Paleozoic rocks older than Ordovician were penetrated. Although Paleogene deposits were the youngest rocks identified, the upper 305 m of the well were not sampled. Inasmuch as shallow stratigraphic test wells (Hathaway and others, 1976) and the COST GE-1 well penetrated Neogene strata, younger deposits are probably present in the uppermost portion of the Transco 1005-1 section.

Inner- to middle-sublittoral, upper and middle Eocene, light-tan to white, micritic, intermittently glauconitic and fossiliferous limestones interbedded with light brown to brown cryptocrystalline, bedded cherts were penetrated between 305 to 863 m. The Upper Cretaceous section is composed of outer-sublittoral Lower Maestrichtian (863 to 908 m), upper-bathyl Campanian (908 to 1174 m), Santonian (1174 to 1247 m), and Coniacian (1247 to 1393 m) light-gray to gray, dense, massive calcareous claystones, and middle-sublittoral to terrestrial Turonian (1393 to 1530 m), light to dark-gray, massive calcareous claystones and siltstones.

Differentiation of the Lower Cretaceous strata within the well is difficult because this portion of the section is mainly nonmarine and dinoflagellates are rare. The terrestrial palynomorphs present could not be used to date this section, not only because of their poor preservation due to the predominance of coarse clastics, but also because the identified forms are known to be present throughout the Early Cretaceous. The sparse dinoflagellates that are present in the red to gray shales, light gray limestones, and well sorted, reddish-brown to light-gray, fine- to medium-grained sandstones between 1530 to 1615 m suggest paralic environments of Albian age. The remainder of the Lower Cretaceous section down to 2667 m is composed of: (1) calcite and hematite cemented, white to reddish-brown, fine- to coarse-grained sandstones; (2) red, green, and gray shales and siltstones; and (3) thin beds of limestone. Traces of coal, anhydrite, gypsum, and pyrite are scatt-

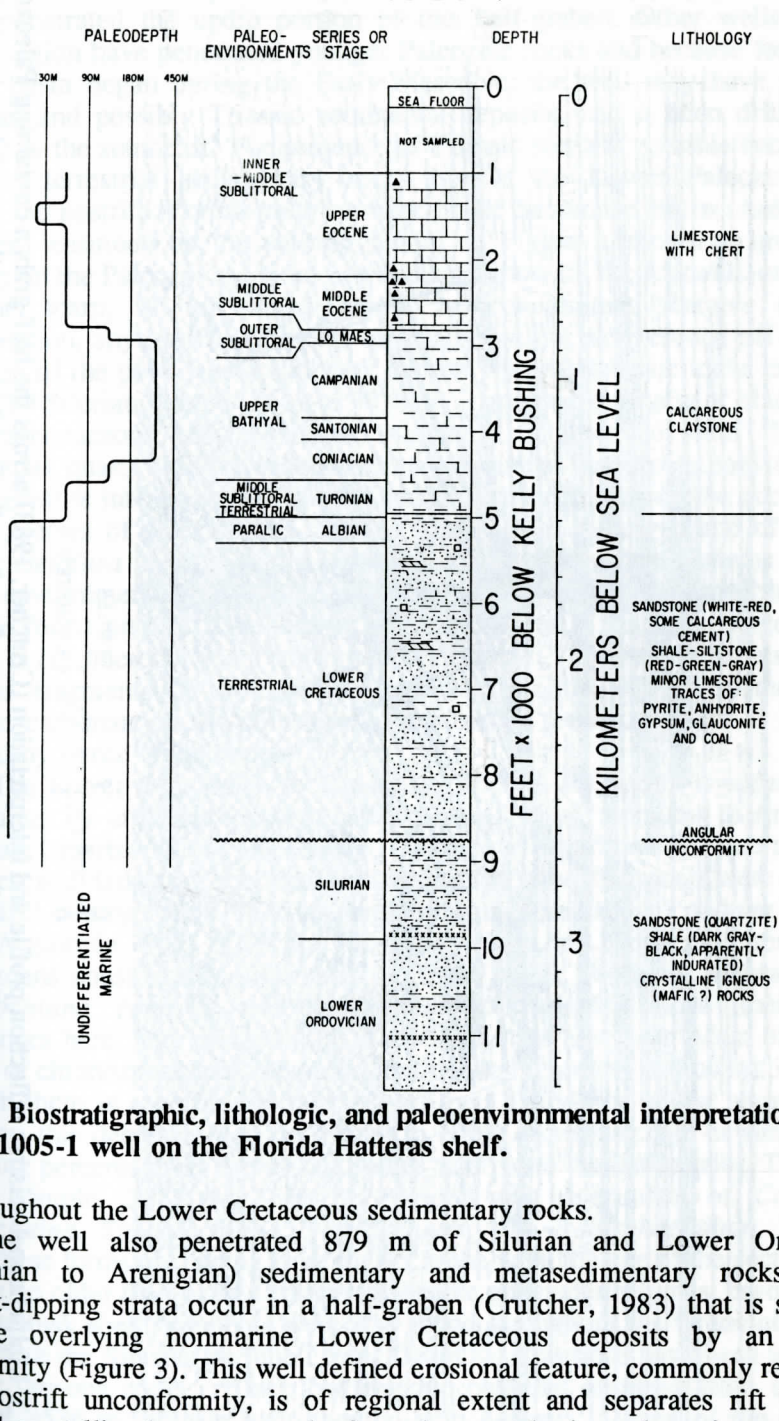

Figure 2. Biostratigraphic, lithologic, and paleoenvironmental interpretation for the Transco 1005-1 well on the Florida Hatteras shelf.

ered throughout the Lower Cretaceous sedimentary rocks.

The well also penetrated 879 m of Silurian and Lower Ordovician (Llanvirnian to Arenigian) sedimentary and metasedimentary rocks. These southeast-dipping strata occur in a half-graben (Crutcher, 1983) that is separated from the overlying nonmarine Lower Cretaceous deposits by an angular unconformity (Figure 3). This well defined erosional feature, commonly referred to as the postrift unconformity, is of regional extent and separates rift basin or deformed crystalline basement rocks from the more horizontal continental-margin rocks. Loose, coarse grains of quartz, recovered in the cuttings from the interval near 2667 m, may represent a lag deposit present at the unconformity surface. The

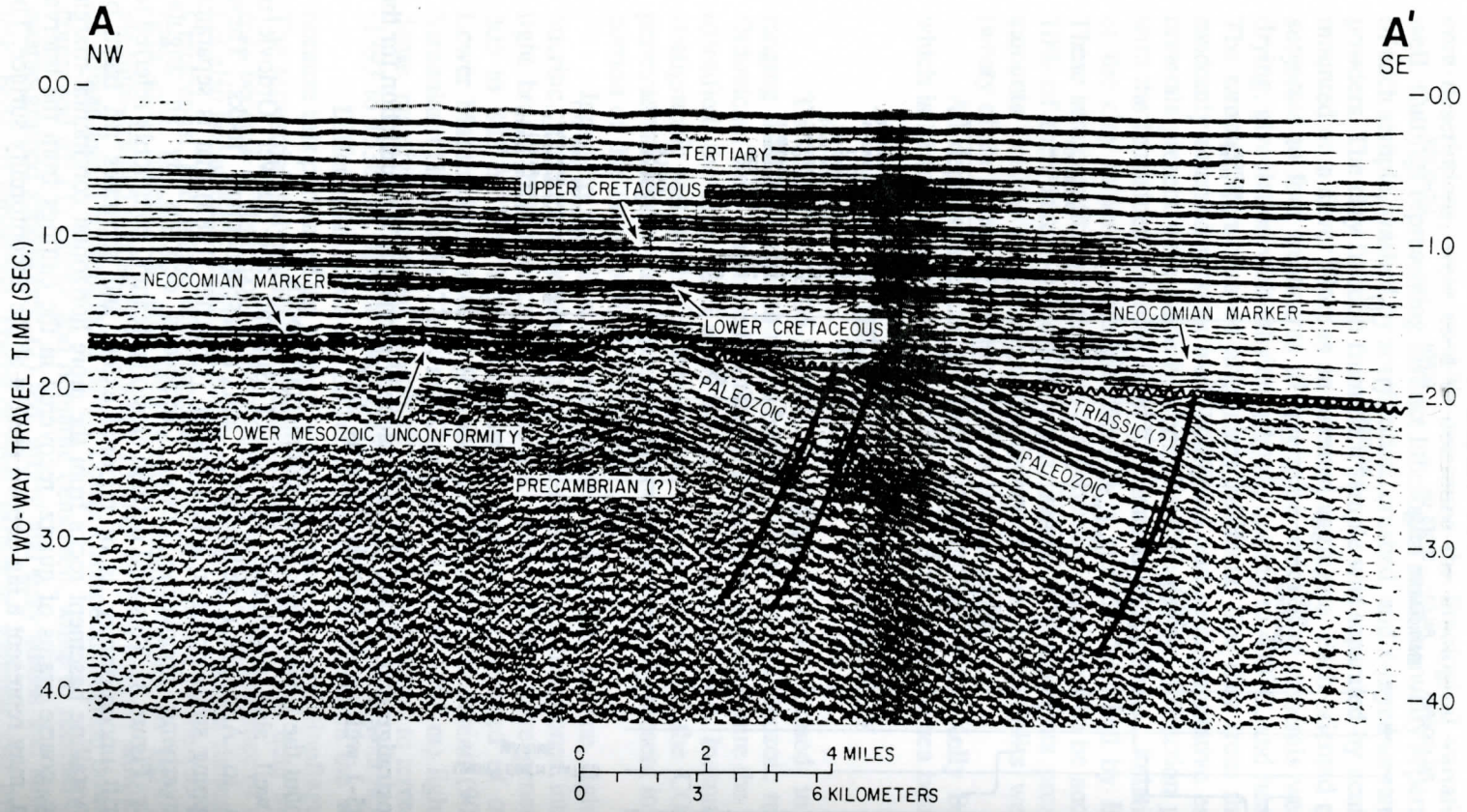

Figure 3. Multichannel seismic reflection profile and interpretation (Crutcher, 1983) across the half-graben containing Paleozoic sedimentary and metasedimentary rocks. These Paleozoic strata are marine, they dip steeply to the southeast, and are separated from nonmarine Lower Cretaceous deposits by an angular unconformity between 1.5 and 2.0 seconds. Because the exact location of the profile could not be accurately determined, the section penetrated by the Transco 1005-1 well has not been superimposed on the profile.

well, which was drilled specifically to test the subconformity play (Breitenwischer, 1981), penetrated the updip portion of this half-graben. Other wells from the general region have penetrated younger Paleozoic rocks and because formation of the rift basin began during the Early Mesozoic, the well may have penetrated Devonian and possibly Triassic continental deposits, had it been drilled farther downdip to the southeast. The presence of Triassic strata is possible because Early Mesozoic terrestrial sedimentary rocks overlie the Lower Paleozoic section beneath the postrift unconformity onshore in the Suwannee Basin (Arden, 1974). However, inasmuch as the seismic record in Figure 3 shows no evidence of downlap on the Paleozoic section, bed thickening toward the footwall, or an eroded fault-line scarp, all of which would be concomitant features of synrift sedimentation, any synrift sediments originally present were eroded off during the formation of the postrift unconformity and only prerift Triassic rocks may remain.

The Silurian section (2667 to 3018 m) is composed largely of black to dark-gray, carbonaceous, fissile shales irregularly interbedded with fine-grained argillaceous quartz wackes, siltstones, quartzarenites, and dolostones (Figure 4). This interval is interpreted as Silurian undifferentiated based on the occurrence of several species of chitinozoans such as *Ancyrochitina ancyrea* and of acritarchs such as *Leiofusa* cf. *bernesgae*. Both the chitinozoans and acritarchs indicate a marine environment of deposition, although no depth interpretation can be made from the forms present. The absence of trilete spores in the assemblage from this interval is considered evidence of pre-Devonian age. The fossil fauna also includes scattered fragments of mollusk shells and graptolites. However, most of the biogenic carbonate in the Silurian portion of the section appears to have been replaced by pyrite or dolomite.

The Lower Ordovician section (3018 to 3546 m), which is separated from the Silurian by an unconformity, consists primarily of medium- to fine-grained, submature quartzarenites interlayered with, and overlain by, quartz wackes, siltstones, and dark-gray, micaceous shales. A few chert fragments were also found in the drill cuttings from 3475 m, suggesting the presence of nodular or bedded chert. A sample from 3018 to 3024 m yielded an excellent assemblage of chitinozoans considerably different from those in the overlying Silurian interval. *Siphonochitina formosa* and *Linochitina* cf. *erratica* have their highest occurrences here, and specimens of *Conochitina* are abundant. Most of the same species of chitinozoans and acritarchs continue to be present downward in the well, although there is a noticeable decrease in their abundance below about 3261 m. However, this decrease may be related to either increasing age or simply to the increasing percentage of barren sandstones relative to the dark shales. The deepest cutting sample, 3527 to 3546 m, yielded rare specimens of *Conochitina*, *Desmochitina*, *Sphaerochitina*, *Veryhachium*, and *Baltisphaeridium*. Therefore, unless these forms are caving from higher in the well, the age of the section at total depth is no older than early Ordovician. Sparse echinoderm spines, bryozoans, and worn mollusk shell fragments were also found throughout the Ordovician section.

Both the Silurian and the Lower Ordovician sections have been intruded by basaltic igneous rocks. Black hydatogenic particles obtained from the drilling fluids at 3536 m indicate hydrothermal vein deposits. Many of the lithologies show signs of incipient (zeolite to greenschist facies) metamorphism related to overburden stresses during burial; there is also evidence for contact metamorph-

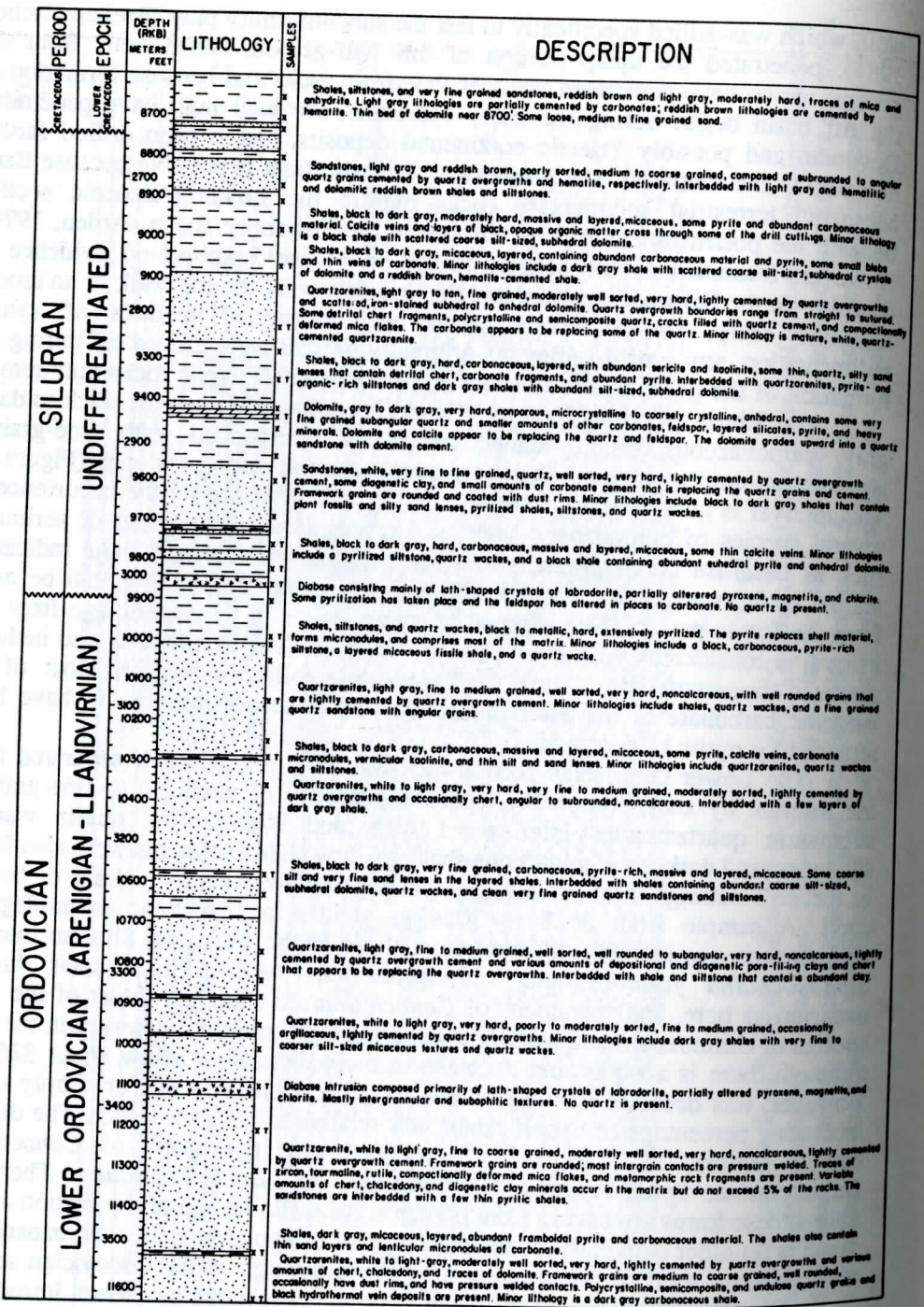

Figure 4. Detailed lithologic descriptions and x-ray powder diffraction (X) and thin section (T) sample locations for the Silurian and Lower Ordovician sections in the Transco 1005-1 well. Lithologic descriptions were determined from the examination of well logs and drill cuttings.

ism associated with the igneous intrusions. Lithologically and mineralogically, this sequence is similar to the black to dark-gray Silurian shales and Lower Ordovician quartzarenites present in the Suwannee Basin beneath the southeastern coastal plain.

MAJOR LITHOLOGIES

Shales

Description: Hard, black to dark-gray, carbonaceous, fissile shales are the predominant lithology in the Silurian and are interlayered with and overlie the quartzarenite sequences in the Ordovician portion of the section. Most of the shales consist primarily of mica flakes and indefinite aggregates of clay, oriented so that the minerals are roughly parallel to the bedding (Figure 5). However, about 44% of the shale cuttings have massive fabrics that correspond to a random orientation and a higher organic content. The shales with the massive fabrics contain scattered, sand-filled burrows and are more common in the Silurian than in the Ordovician section. Regardless of the orientation, many of the mica flakes in the shales have been enlarged by diagenetic recrystallization. This diagenetic enlargement of the individual crystallites has converted textures that were originally silty clays and clayey silts into clayey silts and siltstones, respectively. X-ray diffraction analyses (Table 1) show that the present layered silicate fraction is composed mainly of illite/mica and smaller amounts of kaolinite and chlorite.

The nonclay fraction, which is generally scattered heterogeneously throughout the clay minerals, is also concentrated in distinct, sharply bounded layers. Silt-sized, angular to subangular grains of quartz and feldspar that show little or no signs of alteration comprise most of these thin beds. Authigenic pyrite is present in all of the shales, but in some intervals (notably 3045 to 3048 m) it is a dominant constituent. The pyrite occurs in irregular or rounded masses, single euhedral crystals, framboidal aggregates, and as replacements of shell detritus. Concentrations of organic material within the shales range from traces up to 5%. This carbonaceous organic matter occurs as irregular, individual plant fragments up to about 1.0 mm in diameter, very fine material that cannot be resolved from the matrix, and as black, opaque lenses parallel to the bedding (Figure 6).

Comminuted fossil fragments of calcite, oblate micronodules of siderite, and individual coarse silt- and sand-sized authigenic crystals of calcite, dolomite, and siderite are found scattered throughout many of the shales. The micronodules average about 0.6 mm in length and 0.1 mm in thickness. Reddish-brown shale, which is found in the Silurian section above 2707 m, owes its coloration to hematite, which occurs as finely divided grains and, as a replacement of pyrite, granular crystals. The reddish-brown shale, which decreases in abundance downward within this 40 m thick interval, is interbedded with light-gray and dark-gray shales and medium- to coarse-grained, light-gray to reddish-brown sandstones. The 40 m thickness of the interval is considered a maximum inasmuch as some portion of the reddish-brown cuttings may be downhole cavings from a much thinner sequence.

Comments: The massive fabrics exhibited by many of the shales probably

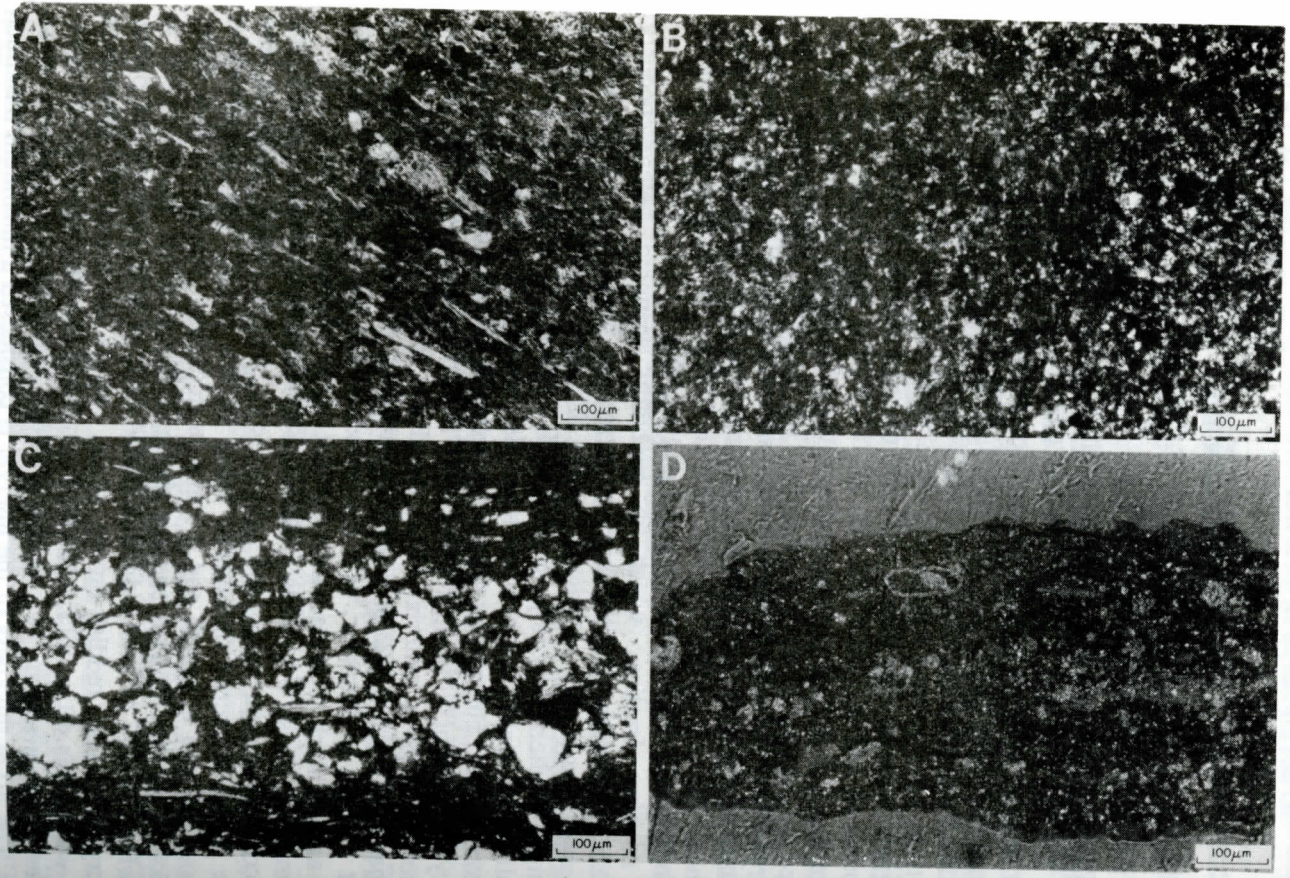

Figure 5. Black to dark-gray, carbonaceous Paleozoic shales from the Transco 1005-1 well. (A) Oriented structure with micaceous minerals roughly parallel to the bedding; 3510 m. (B) Massive, randomly oriented structure due probably to bioturbation; 3226 m. (C) Thin, current-emplaced, silty sand layers within layered shales; 2850 m. (D) Pyritized fossiliferous shale; reflected light, 3047 m.

Table 1. Estimated mineral modes, in relative percent, determined from X-ray diffraction and smear slides for drill cutting samples from the Transco 1005-1 well. SMC: smectite; I-S: mixed layer illite-smectite; CHL: chlorite; I/M: illite/mica; KAO: kaolinite; QTZ: quartz; FLD: feldspar; PYR: pyrite; HEM: hematite; GOE: goethite; MAG: magnetite; SID: siderite; CAL: calcite; ARA: aragonite; D/A: dolomite/ankerite; AMP: amphiboles; PYX: pyroxenes; GYP: gypsum; ANH: anhydrite; EPI: epidote; ANT: antigorite; LG: light gray; RB: reddish brown; BG: blueish gray; DG: dark gray; and G: gray. T <1%. A blank indicates mineral not detected.

SAMPLE METERS RKB	SMC	I-S	CHL	I/M	KAO	QTZ	FLD	PYR	HEM	GOE	MAG	SID	CAL	ARA	D/A	AMP	PYX	COMMENTS
2637-2640		5	6	19	11	19	7	3					21		9			CRET; LG SHALE
2637-2640		8	2	36	3	26	9		11						5			CRET; RB SHALE
2652-2655		6	3	35	5	25	11		T				14		T			CRET; LG SHALE
2652-2655		4	2	36	3	23	11		12				2		8			CRET; RB SHALE
2652-2655		1	T	4	1	19	1						6		67			CRET; DOLOMITE
2661-2664		5	1	39	3	31	6		8						7			CRET; RB SHALE
2682-2685		3	T	28	6	33	5		7						17			SIL; RB SHALE
2704-2707		2	1	28	16	42	6	T	T			T	4					SIL; LG-BG SHALE
2704-2707		2	T	25	4	30	7		25	6								SIL, RB SHALE
2716-2719		T	T	29	23	26	2	16				3			T			SIL; DG SHALE
2716-2719		5	3	28	14	43	5	T	T			T			T			SIL; LG SHALE
2737-2740		T	2	32	16	24	3	21				T			T			SIL; DG SHALE
2765-2768		1	3	33	24	22	1	12				2			2			SIL; DG SHALE
2780-2783		T	T	6	T	86	4	T					T		1	T		SIL; LG QUARTZARENITE
2810-2813			T	7	T	71	4	2				T	6		8			SIL; G QUARTZARENITE
2829-2832			2	37	17	21	5	14				3	1					SIL; DG SHALE
2850-2853			3	29	23	20	6	12				6	T					SIL; B-DG SHALE
2871-2874			1	4	1	88								6				SIL; QUARTZARENITE
2877-2880		T	7	30	14	17	6	3				8	3	1	10			SIL; DG SHALE
2877-2880		T	3	11	8	16	3	1				T	3		54			SIL; DOLOMITE
2887-2890		T	8	25	9	19	6	10				3	3		16			SIL; DG SHALE; GYP=T
2887-2890		T	3	11	13	58		T				2	2		10			SIL; QUARTZARENITE
2911-2914		T	7	35	15	22	7	12				T		T				SIL; DG SHALE; GYP=T
2911-2914			3	9	3	73	7	3				T	1		T			SIL; DG QUARTZARENITE
2926-2929			6	34	15	23	5	13				3	T					SIL; DG SHALE
2926-2929		T	3	7	1	83	T	1						4				SIL; G QUARTZARENITE
2954-2957			2	T	1	95						1						SIL; QUARTZARENITE
2975-2978		T	6	31	19	17	6	15				4						SIL; DG SHALE
2993-2996		T	4	37	12	22	6	15				3	T					SIL; DG SHALE; GYP=T
2993-2996	T	T	5	3	2	81	1						8					SIL; QUARTZARENITE
3005-3008	2		10	T			45	1			12		T			1	28	SIL; DIABASE; EPI=T
3018-3021		1	19	7	11	28	7	7					20					SIL; G-GG SHALE
3018-3021		T	5	30	16	20	6	21				T	T					SIL; DG SHALE
3045-3048		T	3	21	12	15	2	35				T						ORD; DG SHALE; GYP=5; ANH=6
3051-3054				2	T	97		T										ORD; QUARTZARENITE
3063-3066		T	7	32	17	17	4	22				T						ORD; DG SHALE
3063-3066		T		5	1	93	T											ORD; QUARTZARENITE
3094-3097		T	8	25	16	26	4	18				2		T				ORD; DG SHALE
3094-3097				4	T	95												ORD; QUARTZARENITE
3124-3127		T	2	7	1	89												ORD; QUARTZARENITE
3136-3140			3	33	23	18	5	17				T						ORD; DG SHALE
3158-3161		T	3	18	17	18	5	33				3			2			ORD; DG SHALE
3158-3161			T	6	T	93												ORD; QUARTZARENITE
3225-3228			5	23	19	20	3	27				3						ORD; DG SHALE
3240-3243			5	17	16	17	6	35				4						ORD; DG SHALE
3240-3243			T	4	T	95												ORD; QUARTZARENITE
3283-3286			7	23	16	21	4	24				4						ORD; DG SHALE
3283-3286			T	5	T	94												ORD; QUARTZARENITE
3304-3307			T	5	T	94												ORD; QUARTZARENITE
3316-3319			4	31	12	22	5	22				4						ORD; DG SHALE
3338-3341			T	5	T	94												ORD; QUARTZARENITE
3356-3359			5	21	10	27	4	24				3						ORD; DG SHALE
3356-3359			T	7	T	92												ORD; QUARTZARENITE
3383-3386	4		11	T			41				11		T			3	28	ORD; DIABASE; EPI=T; ANT=1
3417-3420			4	20	20	23	5	26				2						ORD; DG SHALE
3447-3450			4	31	14	21	6	21				3						ORD; DG SHALE
3447-3450				4	T	95												ORD; QUARTZARENITE
3475-3478			4	29	15	18	5	25				4						ORD; DG SHALE
3475-3478				3	T	96												ORD; QUARTZARENITE
3509-3511			5	44	11	17	8	13				4						ORD; DG SHALE;
3545-3546			5	34	14	21	9	12				5						ORD; DG SHALE
3545-3546			T	4	T	94												ORD; QUARTZARENITE

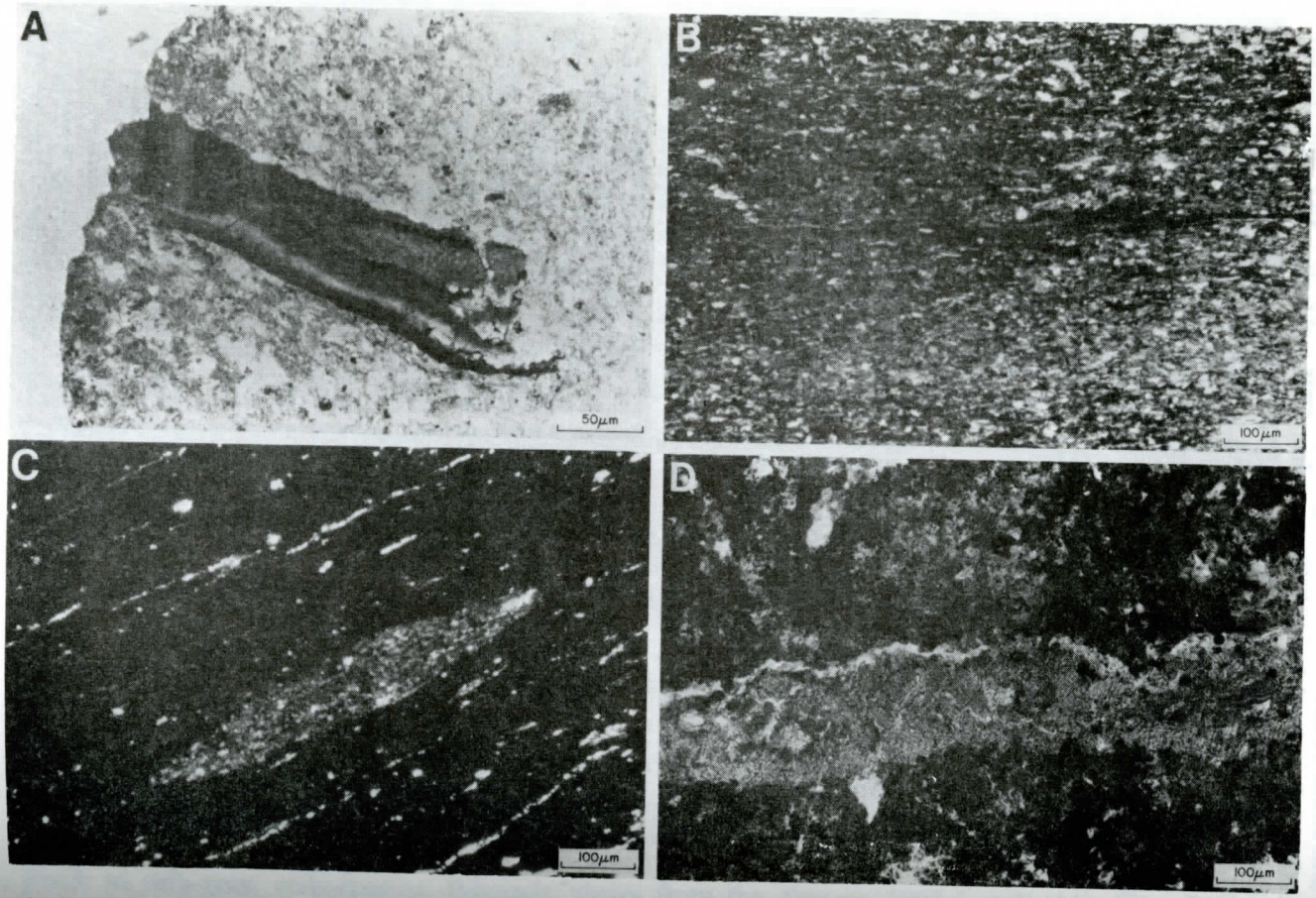

Figure 6. Carbonaceous material and carbonates in the Paleozoic shales. (A) Individual plant fragment; 2926 m. (B) Black, opaque laminae of carbonaceous matter; 2739 m. (C) Compacted, siderite-cemented, quartz sand-filled burrow in a black, carbonaceous shale; 3138 m. (D) Calcite vein, typically found in many of the massive shales; crossed nicols, 2739 m.

indicate active bioturbation, whereas the preservation of bedded fabrics suggests little activity by the benthic infauna (Byers, 1977; O'Brian, 1987). The thinly laminated beds present in the shales with the bedded fabrics were probably emplaced by the sudden changes in depositional conditions associated with stronger currents, possibly associated with storms. The large size and delicate nature of some of the plant fragments present in the shales suggests a shallow-water, low-energy environment. Although most of these shales were probably deposited in a neritic shelf-mud facies, the intervals that are extensively enriched in pyrite suggest deposition under more restricted, anoxic conditions, and the gypsum and anhydrite present in the pyritic interval between 3045 to 3048 m may indicate a lagoonal environment. The occurrence of a paralic environment just below the Lower Ordovician-Silurian unconformity suggests that this hiatus may be due to subaerial erosion. Carrol (1963) attributed the reddish-brown color of the upper portion of the Silurian section beneath Florida to the rapid accumulation of sediment under oxidizing conditions in the absence or near-absence of organic matter. However, because both the Middle Devonian and Silurian strata of northern Florida and Southern Georgia (Pojeta and others, 1976) and the Silurian deposits in the Transco 1005-1 well are oxidized only when immediately beneath the postrift unconformity, the reddish-brown shales are probably alteration products formed during Mesozoic subaerial weathering of the preexistant black shales.

Quartzarenites

Description: Quartzarenites dominate the Ordovician portion of the section and are a major lithology in the Silurian. These quartzarenites are typically white to light-gray and contain medium- to very fine-grained, rounded to subrounded and moderately to well sorted detrital quartz grains (Figure 7). Most of the detrital quartz grains are plutonic and have slightly undulose extinction with some vacuoles and fluid inclusions. Unaligned regular and acicular inclusions are less common. The intergrain boundaries conform to each other suggesting solution effects during diagenetic adjustment. Many contacts between the detrital quartz grains are pressure-welded; some are sutured. Some of the grains exhibit Boehm lamellae or fractures. These fractures may continue across more than one grain and, where tensional movement has occurred, are filled with quartz cement. In rare instances grains are fractured and displaced, but the fractures do not extend into the overgrowth cement. The angular appearance of these grains and the presence of bent or broken muscovite flakes indicates compactional deformation prior to cementation. A general upward progression from mature to submature sandstones is suggested by the decreasing size of the detrital framework grains and increasing sorting values, the angularity of the sand grains, and the volume of matrix within the quartzarenites. The finer grained sandstones tend to contain more angular framework grains, and higher concentrations of detrital clay minerals and mica flakes than the coarser grained sandstones. Faint laminations present in some of the cuttings indicate that some bedding is present.

The quartzarenites are tightly cemented by clear, crystallographically continuous, quartz overgrowths. Contacts between the overgrowths may consist of euhedral terminations (Figure 8), but are commonly irregular compromise

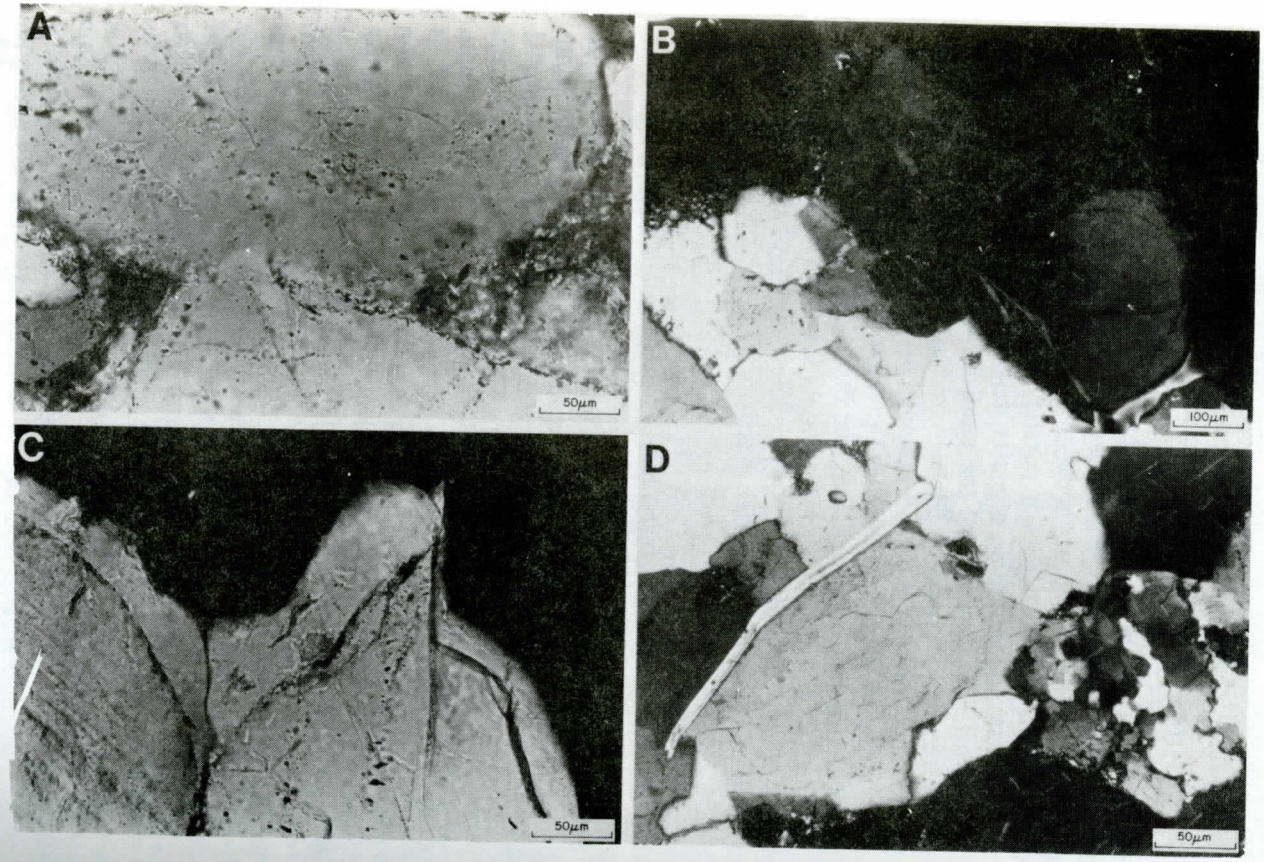

Figure 7. Ordovician quartzarenites from the Transco 1005-1 well. (A) Pressure-welded contact between detrital quartz grains; crossed nicols, 3418 m. (B) Strained detrital quartz grain showing Beohm lamellae; crossed nicols, 3476 m. (C) Fractured and displaced quartz grain where the fracture does not extend into the intergranular quartz cement. Photograph also shows an irregular compromise boundary between the quartz overgrowth cement; crossed nicols, 3476 m. (D) Bent muscovite flake indicating compactional deformation prior to cementation. Detrital grain at right is polycrystalline quartz; crossed nicols, 3095 m.

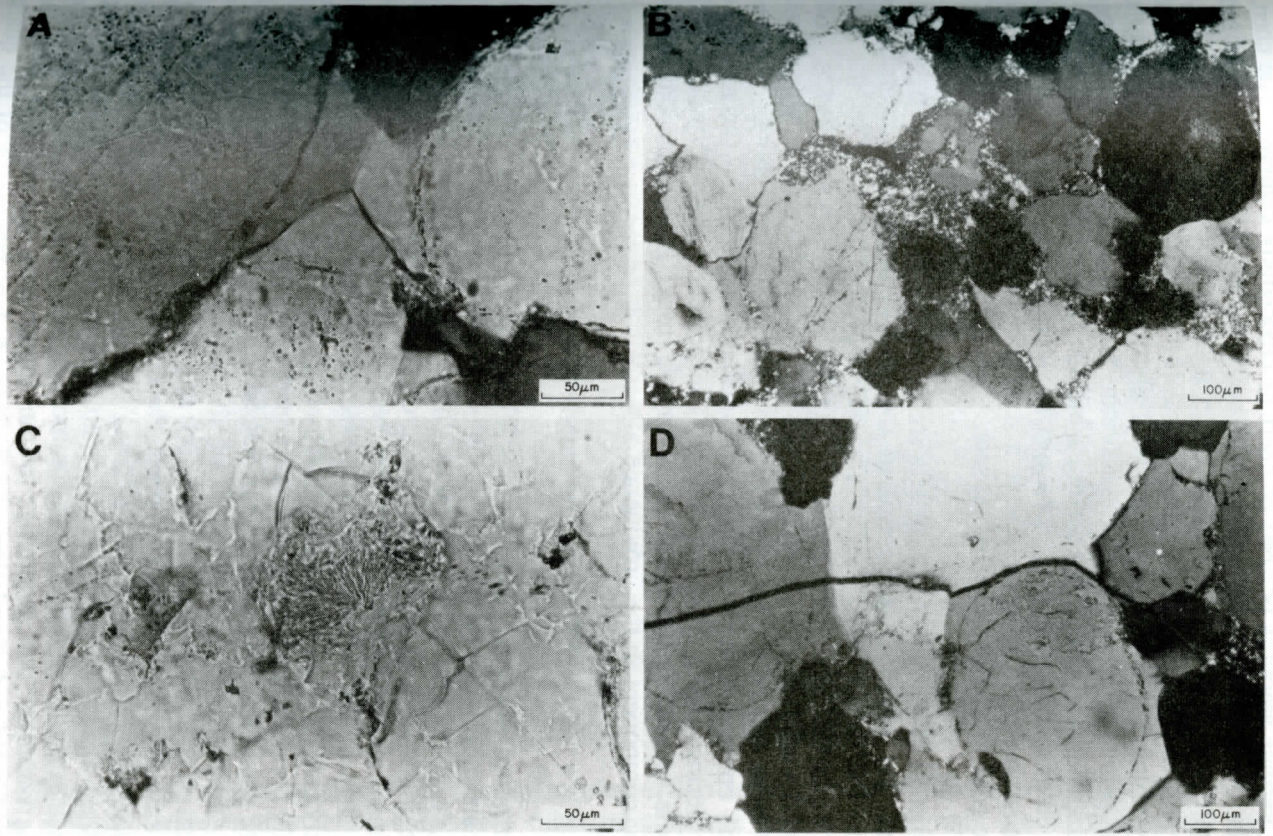

Figure 8. Ordovician quartzarenites from the Transco 1005-1 well. (A) Euhedrally terminated contacts between quartz overgrowths. "Dust rims" show the original surfaces of the detrital quartz grains; crossed nicols, 3114 m. (B) Chert cemented quartzarenite, chert replaces some of the detrital quartz; crossed nicols, 3545 m. (C) Quartzarenite with chalcedony cement; 3545 m. (D) Quartz cement-filled fractures; crossed nicols, 3545 m.

boundaries produced by interference during crystal growth. These overgrowths can usually be distinguished from the detrital grains by "dust rims" that delineate the somewhat dirty surfaces of the original grains. Some of the quartzarenite cuttings also contain various amounts (<20%) of chert or chalcedony cements. The chert, where present, in some instances appears to be replacing the quartz grains and cement. Regardless of the type of cement, little or no pore space remains.

Illite, kaolinite, and chlorite are present in the matrix but are never more than 10% by volume. The irregular interstitial distribution of these clays and the vermicular appearance of some of the kaolinite suggests that they are at least partially authigenic. Detrital heavy minerals include trace amounts of muscovite, biotite, and chlorite flakes and resistate species such as zircon, tourmaline, and rutile. Trace amounts of polycrystalline and semicomposite quartz grains and metamorphic rock fragments are also present.

Comments: The near absence of less stable heavy minerals, rock fragments, and feldspars, the rounded appearance of the detrital quartz and stable heavy minerals, and the depletion of detrital clay suggests that these sediments were extensively winnowed and reworked and may not be first-cycle arenites. The thickness, well-sorted texture, compositional maturity, and sparse, worn fossil contents of these quartzarenites suggests deposition in a high-energy, shallow-water marine environment on a stable continental margin where accumulation could occur during very gradual subsidence. The presence of polycrystalline and semicomposite quartz grains and metamorphic rock fragments indicates a metamorphic component in the provinence.

Siltstones and Quartz Wackes

Description: Siltstones and quartz wackes occur throughout the Paleozoic section, but are more common in the Silurian strata (Figure 9). The siltstones vary from clean, gray-colored rocks composed of angular to subangular, sandy silt-sized quartz grains cemented by quartz overgrowths and chert, to darker quartzose rocks containing an argillaceous matrix that, with an increasing clay content, grade into shales. The quartz wackes are composed of angular to subrounded quartz grains loosely packed in a matrix composed mainly of sericite and chlorite that is at least partially recrystallized. Secondary enlargements of the quartz grains are rare in the quartz wackes. Although feldspar and lithic fragments are always present, they never independently exceed 10% of the granular component. Diagenetic encroachment of the matrix on the framework grains is indicated by green acicular crystals of chlorite that occasionally penetrate into the quartz grains and by the calcite replacement of the quartz and feldspar grains. Many of the feldspar grains have also been altered by seritization, vacuolization, and kaolinization. Quartz and carbonate cements are much less common in the quartz wackes than in the cleaner quartzarenites due primarily to the impervious matrix that fills the interstices and restricted circulation of solutions. A few fragments of the quartz wackes, especially near 3045 m, have been extensively pyritized. In these cuttings, the pyrite has replaced the matrix and appears to be replacing the quartz grains and cement. Oolites of pyrite consisting of concentric laminations of pyrite and anhydrite or pyrite and quartz, occur near 3010 m. Small amounts of quartz

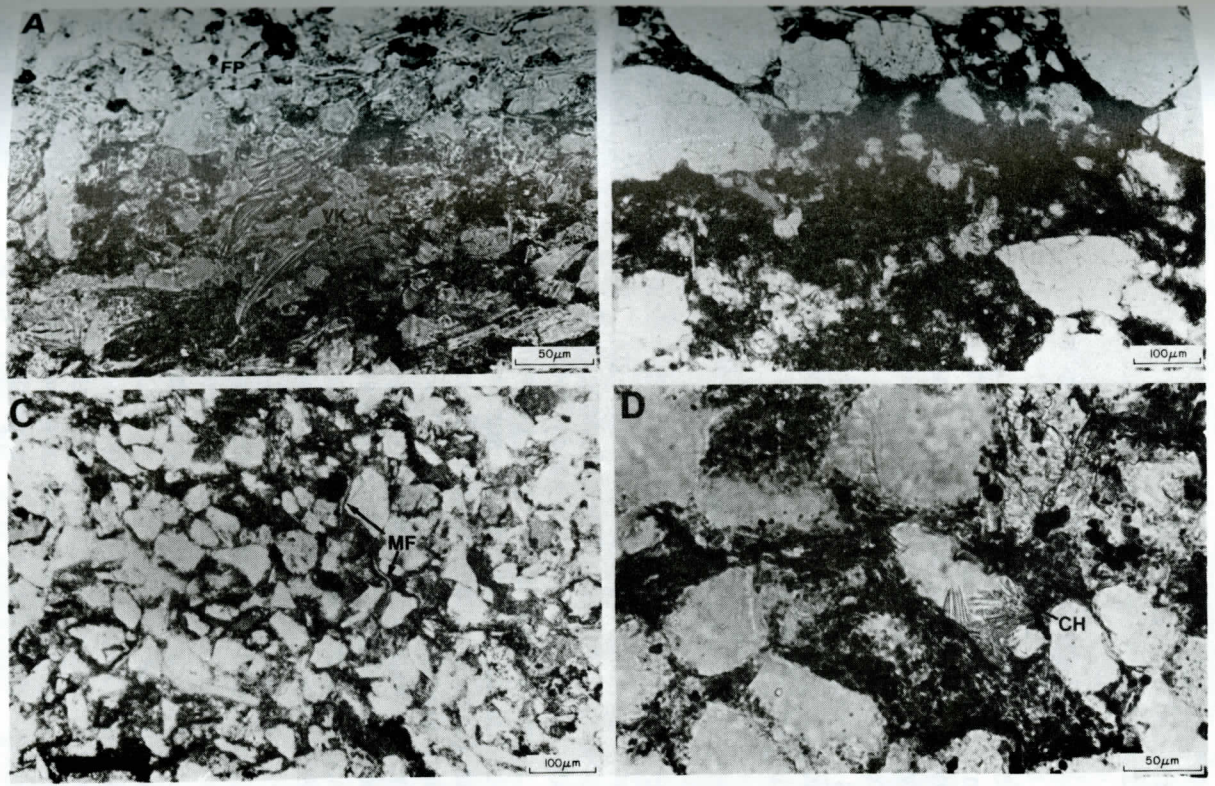

Figure 9. Siltstones and quartz wackes from the Paleozoic section in the Transco 1005-1 well. (A) Relatively clean sandy, Ordovician siltstone composed of chert-cemented, subangular quartz grains. Photograph shows framboidal pyrite (FP) and vermicular kaolinite (VK); 3138 m. (B) Silurian quartz wacke composed mainly of subrounded to subangular quartz grains in a matrix of sericite and chlorite; 2975 m. (C) Silurian quartz wacke composed mainly of angular to subangular quartz grains. Photograph shows bent mica flakes (MF); 2993 m. (D) Diagenetic chlorite crystals (CH) penetrating a detrital quartz grain within a Silurian quartz wacke; 2993 m.

overgrowth and chert cement are sometimes present in the quartz wackes. Flaser bedding, which implies that both sand and mud were available (Reineck and Wunderlich, 1968), is present in some of the Silurian siltstone and fine-grained quartz wacke cuttings.

Both the siltstone and quartz wackes are very hard and contain scattered detrital mica flakes. These flakes of muscovite and biotite usually have a pronounced orientation parallel to the bedding plane.

Comments: These quartz wackes suggest either an increase in the accumulation rate due to greater subsidence and sediment input, an increase in the fine fraction of the source sediments, or a change in depositional environment to that of a transitional zone (Reineck and Singh, 1973) between coastal sands and shelf-mud sediments. In any case, under these conditions the more rapid rate of burial precludes extensive winnowing during transport and deposition. Deposition of the quartz wackes in a deeper-water, slope facies is unlikely because faunal and floral assemblages present in the Silurian of Florida, which would be seaward of the well site on the Iapetus continental margin, suggest an essentially shallow sea dotted with flat lying islands or shoals (Cramer, 1973).

Dolostones

Description: Nonporous dolostones, sandy dolostones, and packed, dolomitic quartzarenites interbedded with dark-gray shales were penetrated between 2874 to 2880 m (Figure 10). The dolostones and shales are more common in the lower portion of this interval; the sandy dolostones and packed dolomitic quartzarenites are more common in the upper portion. The dolomite is commonly anhedral, but subhedral to rhombic forms are recognizable within the matrix. Patches of poikilotopic cement are present, but most of the detrital grains are cemented by medium-grained, equant crystals of dolomite. Larger aggregates (0.1 to 0.3 mm) of anhedral dolomite are probably the remains of dolomitized fossils. Unfortunately, the original fossils, textures, and structures have been masked by the subsequent dolomitization. The dolomite is also associated with small amounts of calcite and siderite. The calcite, which is irregularly distributed and comprises up to 25% of the carbonate in a few of the drill cuttings, occurs as ghosts of an earlier cement and is generally absent or present only in trace amounts. However, small veins of calcite also cut individual dolomite crystals and pseudomorphic rhombs of calcite after dolomite suggest that at least some of this calcite is a late replacement of the dolomite.

The detrital clastic fraction in the dolomitic interval is composed mainly of very fine sand-sized to coarse silt-sized, subangular to angular, moderately well sorted grains of quartz and feldspar. Many of these quartz and feldspar grains are partly replaced by the dolomite; some are partly replaced by calcite. Quartz overgrowths, where they occur, pre-date the carbonate cementation. Illite, kaolinite, smaller amounts of chlorite, and trace amounts of mica flakes, polycrystalline quartz grains, chert fragments, and heavy minerals are also present.

Comments: Although dolomite may form by primary precipitation under specific conditions and dolomitic cement with floating quartz grains may evolve

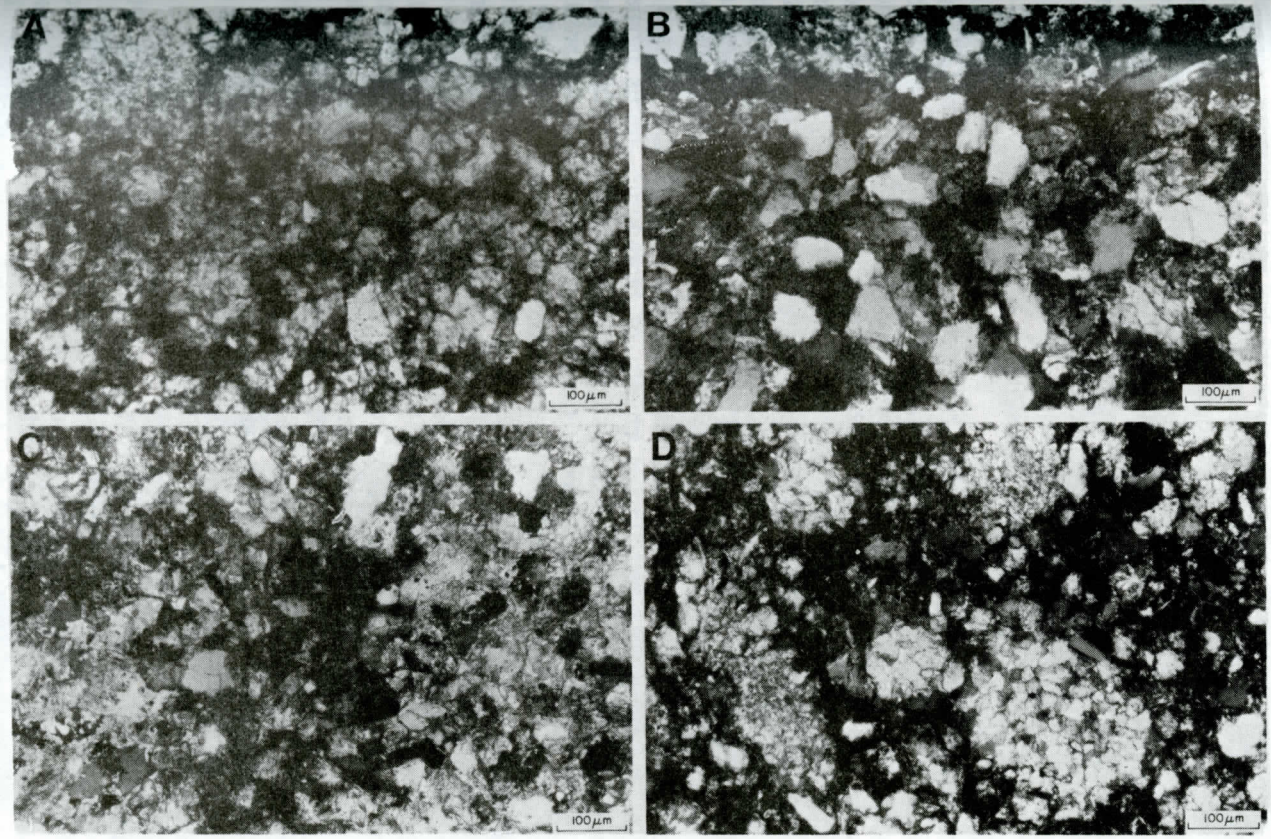

Figure 10. Dolomitic rocks from the Silurian section of the Transco 1005-1 well. (A) Dolostone; 2879 m. (B) Packed, dolomitic quartzarenite in which some of the detrital grains are being replaced by dolomite; crossed nicols, 2879 m. (C) Patch of poikilotopic cement in a dolostone; crossed nicols, 2879 m. (D) Fossil crinoid occicles/columnals (?) replaced by dolomite in a dolostone; crossed nicols, 2879 m.

from the recrystallization of detrital grains of dolomite (Land, 1983), most of the dolomite in this interval formed as a diagenetic replacement product of the original shell material or calcite cement. Variable carbonate and detrital fraction contents within individual, and between different, drill cuttings are probably related to the occurrence and distribution of this original shell material, but it may also be associated with the with the progressive replacement of silicates by carbonate. Inasmuch as many of the detrital silicate grains exhibit evidence of replacement, it is conceivable that this process could have continued until rocks that were originally calcareous quartzarenites were converted into the dolomites.

Igneous Intrusions

Description: Diabase intrusions were penetrated in two intervals (3001 to 3008 m and 3382 to 3391 m) within the well, but the presence of sparse chips of basaltic rock fragments from 3307 and 3539 m suggest other thinner igneous intrusions were also encountered. Most of the drill cuttings have intergranular or subophitic textures, but a few fragments exhibiting intersertal and ophitic texture were also found. Many of the observed changes in the size and composition of the constituent crystals of these different textures are probably related to differential cooling and settling within the intrusions. The diabase, which was emplaced as either shallow dikes or sills, is tholeiitic, dark greenish-gray, and, with the exception of the rare intersertal fragments, holocrystalline (Figure 11). No quartz is present. The plagioclase, which consists chiefly of labradorite, forms tabular, simply twinned (Carlsbad ?), unzoned, lath-shaped euhedral crystals that average about 0.47 mm in length. The clinopyroxene is mostly augite that has been partially altered to chlorite (chlorophaeite) and small amounts of antigorite. Some chlorite is found as radiating fibrous pseudoamygdules that have grown by progressive replacement of the surrounding pyroxene (Figure 12). Chlorite is also found disseminated throughout the groundmass. Opaque minerals make up about 10% of the samples. Magnetite (average 0.1 mm) is found as octahedra and irregular patches; small amounts of pyrite occur in the intrusion near 3005 m. Skeletal crystals of ilmenite are found in the intrusion near 3386 m, and scattered granules of leucoxene, which are probably an alteration product of ilmenite, are found in both intrusions. Secondary calcite occurs as finely disseminated crystals within the groundmass and as a replacement in laths of plagioclase. Trace amounts of lamprobolite, orthopyroxene (hypersthene), biotite, olivine, and slender needles of chlorapatite are also present.

Comments: Diabase, basalt, and rhyolite intrusions, associated with Paleozoic, Triassic, and Jurassic rocks, have been reported from over 50 wells in the coastal plain of Alabama, northern Florida, and southeastern Georgia (Milton and Hurst, 1965; Bass, 1969, and Daniels and others, 1983). Although the diabases penetrated in the Transco 1005-1 well could not be dated, mineralogically similar intrusions in the Paleozoic sedimentary rocks beneath northern Florida give dates between 180 to 190 Ma (Grasly and Wilson, 1967; Lanphere, 1983) and suggest that both occurrences are related to early Mesozoic rifting.

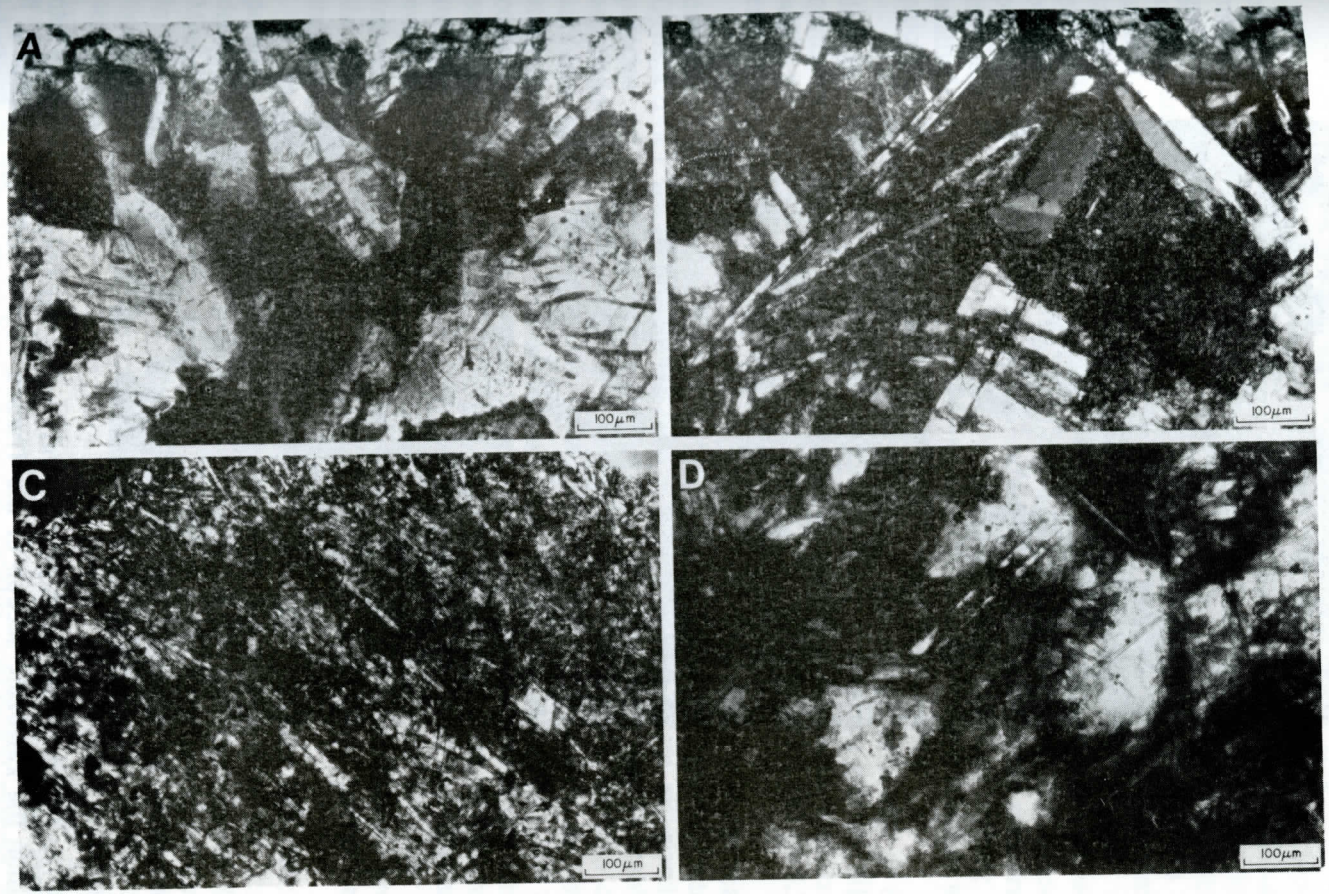

Figure 11. Textures from the Mesozoic igneous intrusion in the Ordovician section of the Transco 1005-1 well. (A) Sectioned igneous cutting with an intergranular texture; 3385 m. (B) Igneous cutting showing a subophitic texture; crossed nicols, 3385 m. (C) Igneous cutting showing an intersertal texture; crossed nicols, 3385 m. (D) Igneous cutting with an ophitic texture; 3385 m.

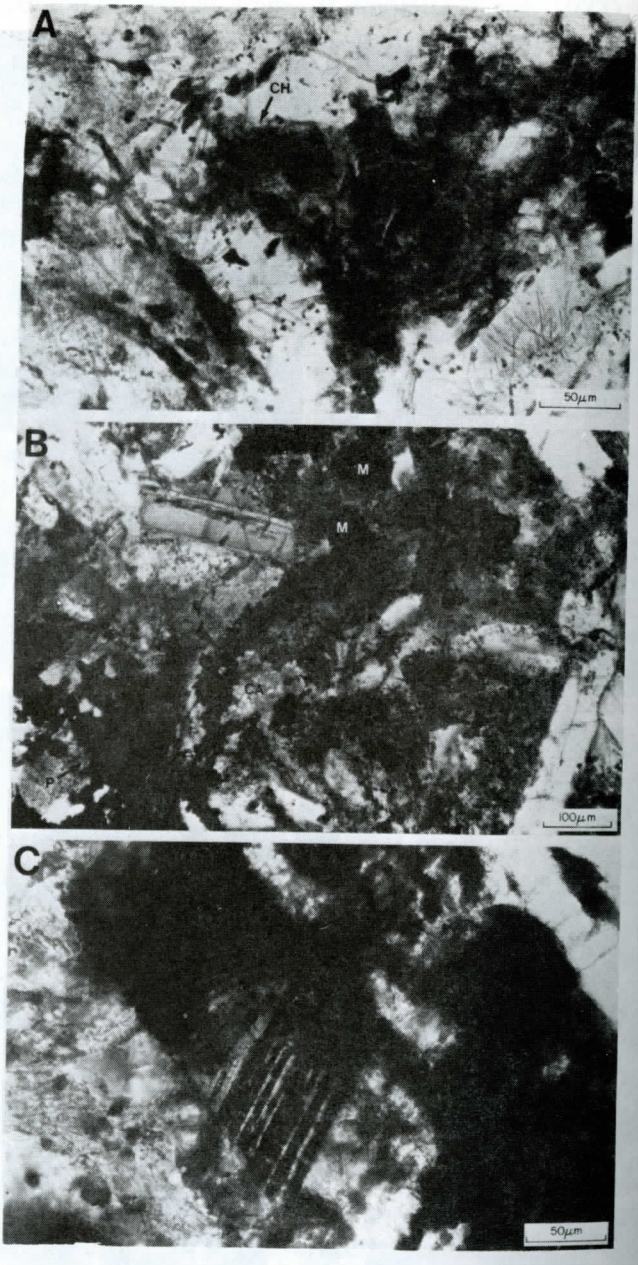

Figure 12. Hydrothermal alteration and opaque minerals in the diabase intrusions within the Paleozoic section of the Transco 1005-1 well. (A) Radiating, fibrous pseudoamygdules of chlorite (CH) replacing partially altered pyroxene; Ordovician, 3385 m. (B) Pyrite (P) and subhedral magnetite (M) in an ophitic drill cutting, calcite (CA) is replacing a lath of plagioclase; Silurian, 3007 m. (C) Skeletal crystal of ilmenite; crossed nicols, Ordovician, 3385 m.

SUMMARY

The well, drilled to 3,546 m RKB in the Southeast Georgia Embayment, penetrated 879 m of Silurian and Lower Ordovician sedimentary and metasedimentary rocks. These strata dip steeply to the southeast and occur in a half-graben separated from the overlying nonmarine Lower Cretaceous deposits by an angular unconformity. The lithology of the Paleozoic section suggests a general upward progression from neritic or littoral sands to lower energy shelf-mud and lagoonal deposits. The Ordovician section (3,018 to 3,546 m) consists predominantly of medium- to fine-grained quartzarenites interlayered with and overlain by quartz wackes, siltstones, and dark-gray shales. The presence of polycrystalline and semicomposite quartz grains and metamorphic rock fragments indicates a metamorphic component in the provenance; low sorting values, relatively simple mineralogy, and rounding of the resistate heavy minerals suggests processes involving extensive transport and sustained reworking.

The Silurian section (2,667 to 3,018 m) is composed primarily of black to dark-gray, carbonaceous, fissile shales interbedded with quartz wackes, siltstones, quartzarenites, and dolostones. Diabase intrusions of probable Mesozoic age, which were penetrated in two intervals (3,001 to 3,008 m and 3,382 to 3,391 m), exhibit intergranular to subophitic textures.

The lithology and internal fabric of the Lower Paleozoic rocks indicates that deposition of the sediments took place mainly in shallow epicontinental seas. Quartzarenites and carbonaceous shales containing abundant silt-sized quartz particles are characteristic lithologies of subenvironments within stable shelf associations; dolomitization of carbonates and secondary chert are also common attributes. Furthermore, the 1005-1 well Lower Paleozoic section, as with most stable shelf associations, is also marked by numerous disconformities, low feldspar concentrations, and relatively thin sequences. Shales and immature sandstones scattered throughout and overlying the clean, Ordovician quartzarenites represent transgressive events; the unconformity between the Ordovician and Silurian strata, evaporite-bearing shales, and mature sandstones within the Silurian indicate regressive periods. The thin-bedded, fine-grained immature sandstones present in the Silurian were probably emplaced by changes in sediment source or storm-induced currents.

The lithology, mineralogy, and stratigraphy of the Lower Paleozoic section penetrated by the Transco 1005-1 well is strikingly similar to the Paleozoic deposits found beneath the coastal plain strata of the southeastern U.S., in Morocco, Senegal, and Guinea, West Africa, and in the Amazon and Parana Basins in Brazil. Lithologic differences, such as the presence of dolostones and extensively pyritized shales containing gypsum and anhydrite in the Silurian section of the Transco well, are probably related to facies changes associated with lateral variation in depositional conditions. If, as discussed earlier, the Lower Paleozoic sections beneath the southeastern United States and West Africa were deposited on the African-South American, Iapetus continental margin, then the lithologically similar and more centrally located Lower Ordovician and Silurian strata in the Transco 1005-1 well and the Middle Devonian rocks in the COST GE-1 well were deposited on the same margin and subjected to similar depositional and diagenetic conditions.

ACKNOWLEDGEMENTS

We thank P. Popenoe and D.W. O'Leary for reviewing this manuscript and Transco Exploration, Inc. for providing the drill cuttings used during this study. Paleontologic analysis of the well was performed by International Biostratigraphers, Inc. under contract to Transco Exploration, Inc. The biostratigraphic and lithologic information presented in Figure 2 are available from the National Geophysical Data Center, in Boulder Colorado.

REFERENCES CITED

Applin, P.L., 1951, Preliminary report on the buried pre- Mesozoic rocks in Florida and adjacent states: U.S. Geol. Sur. Circ. 91, 28 p.

Arden, D.D., 1974, A geophysical profile in the Suwannee Basin, Northwestern Florida: *in* Stafford, L.P. (ed.), Symposium on the Petroleum Geology of the Georgia Coastal Plain, Georgia Dept. Natrl. Resources Bull. 87, p. 111- 122.

Bass, M.N., 1969, Petrography and ages of crystalline basement rocks of Florida- some extrapolations: *in* Other Papers on Florida and Brittish Honduras, Amer. Assoc. Pet. Geol. Mem. 11, p. 283-310.

Biscaye, P.E., 1965, Mineralogy and sedimentation of recent deep-sea clay in the Atlantic Ocean and adjacent seas and oceans: Geol. Soc. Amer. Bull., v. 76, no. 7, p. 803- 832.

Breitenwischer, R.H., 1981, Frontier exploration- Southeast Georgia Embayment: Amer. Assoc. Pet. Geol., v. 65, no. 9, p. 1659.

Byers, C.W., 1977, Biofacies patterns in euxinic basins: a general model: Soc. Econ. Paleo. Min. Spec. Publ. 25, p. 5-17.

Carrol, D., 1963, Petrography of some sandstones and shales of Paleozoic age from borings in Florida: U.S. Geol. Sur. Prof. Paper 454, A1-A15.

Chowns, T.M. and Williams, C.T., 1983, Pre-Cretaceous rocks beneath the Georgia coastal plain- regional implications: *in* Gohn, G.S. (ed.) Studies related to the Charleston, South Carolina earthquake of 1886- Tectonics and Seismicity, U.S. Geol. Sur. Prof. Paper 1313, L1-L42.

Cook, F.A., and Oliver, J.E., 1981, The Late PreCambrian edge in the Appalachian Orogen: Amer. Jour. Sci., v. 281, p. 993-1008.

Cramer, F.H., 1971, Position of the north Florida Lower Paleozoic block in Silurian time: Jour. Geophy. Res., v. 76, no. 20, p. 4754-4757.

Crutcher, T.D., 1983, Southeast Georgia Embayment: *in* Bally, A.W. (ed), Seismic Expression of Structural Styles- A Picture And Work Atlas, Amer. Assoc. Pet. Geol., Tulsa, p. 2.2.3-27-2.2.3-29.

Dallmeyer, R.D., 1987, Ar40/Ar39 age of detrital muscovite within Lower Ordovician sandstone in the coastal plain basement of Florida: implications for west African terrane linkages: Geology, v. 15, p. 998-1001.

Daniels, D.L., Zietz, I., and Popenoe, P., 1983, Distribution of subsurface Lower Mesozoic rocks in the southeastern United States, as interpreted from regional aeromagnetic and gravity maps: *in* Gohn, G.S. (ed.) Studies related to the Charleston, South Carolina earthquake of 1886- Tectonics and Seismicity, U.S. Geol. Sur. Prof. Paper 1313, p. K1-K24. Dillon, W.P. and Sougy, J.M.A., 1974, Geology of West Africa and Canary and Cape Verde

Islands: *in* Nairn, A.E.M. and Stehli, F.G. (eds.), The Ocean Basins and Margins, Plenum Press, New York, p. 315-390.
Dillon, W.P. and Popenoe, P., 1988, Development of the continental margin in the southeastern United States- the Blake Plateau and Carolina Trough: *in* Sheridan, R.E. and Grow, J.A. (eds.) The Atlantic Continental Margin: U.S., The Geology of North America, v. I-2, Geol. Soc. Amer., Boulder, CO, p. 291-327.
Grasty, R.L. and Wilson, J.T., 1967, Ages of Florida volcanics and the Opening of the Atlantic Ocean: T. Amer. Geophy. Union, v. 48, p. 212-213.
Gunter, H., 1928, Basement rocks encountered in a well in Florida: Amer. Assoc. Pet. Geol., v. 12, p. 1107-1108.
Hathaway, J.C., Schlee, J.S., Poag, C.W., Valentine, P.C., Weed, E.G., Bothner, M.H., Kohout, F.A., Manheim, F.T., Schoen, R., Miller, R.E., and Schultz, D.M., 1976, Preliminary summary of the 1976 Atlantic Margin Coring Project of the U.S. Geological Survey: Open-File Rept. No. 76-844, 218 p.
Hutchinson, D.R., Klitgord, K.D., and Detrick, R.S., 1986, Rift basins of the Long Island Platform: Geol. Soc. Amer. Bull., v. 97, p. 688-702.
Klitgord, K.D. and Schouten, H., 1987, Constraints imposed by plate tectonics on the geometry and time of opening of the Gulf of Mexico: Geol. Soc. Amer., Abs. Prog., v. 19, no. 7, p. 729.
Klitgord, K.D., Hutchinson, D.R., and Shouten, H., 1988, U.S. Atlantic continental margin; structural and tectonic framework: *in* Sheridan, R.E. and Grow, J.A. (eds.) The Atlantic Continental Margin: U.S., The Geology of North America, v. 1-2, Geol. Soc. Amer., Boulder, CO, p. 19-55.
Land, L.S., 1983, Dolomitization: Amer. Assoc. Pet. Geol., Note Series 24, 20 p.
Lanphere, M.A., 1983, Ar40/Ar39 ages of basalts from Clubhouse Crossroads Test Hole #2, near Charleston, South Carolina: *in* Gohn, G.S. (ed.) Studies related to the Charleston, South Carolina earthquake of 1886- Tectonics and Seismicity, U.S. Geol. Sur. Prof. Paper 1313, p. B1-B8.
Milton, C. and Hurst, V.J., 1965, Subsurface "basement" rocks of Georgia: Georgia Geol. Sur. Bull. No. 76, 56 p.
Neathery, T.L. and Thomas, W.A., 1975, Pre-Mesozoic basement rocks of the Alabama Coastal Plain: Trans. Gulf Coast Assoc. Geol. Soc., v. 25, no. 1, p. 86-99.
Nelson, K.D., Arnow, J.A., McBride, J.H., Willemin, J.H., Huang, J., Zheng, L., Oliver, J.E., Brown, L.D., and Kaufman, S., 1985, New COCORP profiling in the southeastearn United States. Part I: Late Pelaozoic suture and Mesozoic rift basin: Geology, v. 13, p. 714- 718.
O'Brien, N.R., 1987, The effects of bioturbation on the fabric of shales: Jour. Sed. Pet., v. 57, no. 3, p. 449- 455.
Opdyke, N.D., Jones, D.S., MacFadden, B.J., Smith, D.L., Mueller, P.A., and Shuster, R.D., 1987, Florida as an exotic terrane: Paleomagnetic and geochronologic investigation of Lower Paleozoic rocks from the subsurface of Florida: Geology, v. 15, p. 900-903.
Petters, S.W., 1979, West African cratonic stratigraphic sequences: Geol., v. 7, p. 528-531.
Pojeta, J., Kriz, J., and Berdan, J.M., 1976, Silurian- Devonian pelecypods and Paleozoic stratigraphy of subsurface rocks in Florida and Georgia and

related Silurian pelecypods from Bolivia and Turkey: U.S. Prof. Paper 879, p. 1-29.
Reineck, H.E. and Wunderlich, F., 1968, Classification and origin of flaser and lenticular bedding: Sediment., v. 11, no. 1, p. 99-104.
Reineck, H.E. and Singh, I.B., 1980, Depositional Sedimentary Environments: Springer-Verlag, New York, 549 p.
Rhodehamel, E.C., 1979, Lithologic descriptions: in Scholle, P.A. (ed.) Geological studies of the COST GE-1 well, United States South Atlantic Outer Continental Shelf area, U.S. Geol. Sur. Circ. 800, p. 24-36.
Smith, D.L., 1982, Review of the tectonic history of the Florida basement: Tectonophys., v. 88, p. 1-22.
Sougy, J.M.A., 1962, West African Fold Belt: Geol. Soc. Amer. Bull., v. 73, p. 871-876.